Draft version 0.3

ATLAS NOTE

January 16, 2017

Search for Higgs pair production with decays to WW(jjjj) and $\gamma\gamma$ in 36.5 fb^{-1} proton-proton collision data at 13 TeV in the ATLAS detector

ATLAS Collaboration[1], Yu Zhang[1], Jin Wang[2.], Jason Veatch[3.], Kai Henßen[3.], Stan Lai[3.]

[1.] *Institute of High Energy Physics, Chinses Academy of Siences, Beijing, China*
[2.] *University of Sydney, Sydney, Australia*
[3.] *II. Physikalisches Institut, Georg-August-Universität, Göttingen, Germany*

Abstract

A search is performed for resonant and non-resonant Higgs pair production with one Higgs boson decaying to full hadronic WW^* and the other to $\gamma\gamma$ using proton-proton collision data corresponding to an integrated luminosity of 36.5 fb^{-1} at a 13 TeV centre-of-mass energy recorded with the ATLAS detector. No deviation from the Standard Model prediction is observed. The observed (expected) upper limit at 95% confidence level on the cross section for $gg \to hh$ is XXX pb (XXX pb) for the non-resonant Higgs pair production. For resonant Higgs pair production, the observed (expected) upper limits at 95% confidence level on cross section times the branching ratio of $X \to hh$ range from XXX pb (XXX pb) to XXX pb (XXX pb) as a function of the resonant mass from 260 GeV to 500 GeV assuming that the narrow-width approximation holds.

© Copyright 2017 CERN for the benefit of the ATLAS Collaboration.
Reproduction of this article or parts of it is allowed as specified in the CC-BY-3.0 license.

Contents

1 Statements

1.1 version 0.0

22.1 fb^{-1} of data and 260 GeV signal sample are used for first selection optimization.
To do list:

- optimize the jet combination. Selecting leading 4 or 3 jets is not the optimal strategy.
- check signal of other mass point and investigate more kinematic variables for further selection optimization.
- signal and background modeling.
- systematics study.

1.2 version 1.0

- further discuss the selection optimization but still keep the baseline selection
- boosted analysis will not go to Moriond2017
- We need to fix the problem of spurious signal and determine the final background modeling.
- The experimental systematics will come soon.

2 Introduction

The discovery of Higgs boson in 2012 [1, 2] by the ATLAS and CMS collaboration at the LHC is a victory of the mechanism of electroweak symmetry breaking (EWSB) and it opened a new door to test the boson sector of the Standard Model (SM). The further studies of the Higgs boson coupling to fermions and bosons as well as the measurments of the spin and parity properties show the consistency with the the prediction of the SM[3, 4, 5]. The measurement of the self-coupling of the Higgs boson is also crucial to test the mechanism of EWSB. Due to their expected small cross sections predicted by the SM [6, 7, 8], this measurement is sensitive only at the high luminosity LHC. However, some beyond SM such as Minimal Supersymmetric Standard Model (MSSM) [9], Two Higgs doublet (2HDM) [10] can potentially boost the production rate. With these models, a heavy CP-even Higgs can decay into two SM Higgs (h) which leads to a resonant search in comparison to the non-resonant one as SM predicts.

Both the ATLAS and CMS collaborations have extensively searched for resonant and non-resonant higgs pair production [11, 12, 13, 14]. The results of the decay channels of $hh \to bbbb$, $hh \to \gamma\gamma bb$, $hh \to \gamma\gamma WW^* \to \gamma\gamma l\nu qq$ and $hh \to bb\tau\tau$ have been published by ATLAS. In this note, the search for $hh \to \gamma\gamma WW^*$ with both W decaying hadronically has been reported. The resonance mass m_H considered in this paper ranges from 260 GeV to 500 GeV. In contrast to $\gamma\gamma l\nu qq$ final state, this channel has higher signal rate but more QCD backgrounds. different Kinematic variables are investigated to further suppress QCD backgrounds.

This paper is organized as follows. Data and Monte Carlo (MC) samples are described in Sec. 3 and the object reconstruction and identification are outlined in Sec. 4. The analyses including event selection and further optimization are presented in Secs. 5 and 6, respectively. The signal modeling and background estimation are discussed in Sec. 7. Different source of uncertainties from both experimental and theoretical sides are summarized in Sec. 8. The statistical and combination procedure between $\gamma\gamma 3j$ and $\gamma\gamma 4j$ categories is described in Sec. 9. Finally, the results of the analyses are reported in Sec. 11.

3 Data and Monte Carlo samples

3.1 Data samples

The data samples used in this analysis correspond to the data recorded by ATLAS in the whole 2015 (3.2 fb^{-1}) and 33.3 fb^{-1} of 2016, which sums up to an integrated luminosity of 36.5 fb^{-1}. The whole dataset is recorded with all subsystems of ATLAS operational [1].

3.2 Monte Carlo samples

SM single Higgs bacgkrounds and signals are estimated with MC samples that are documented in this section, while the continuum photon background of the SM processes with multiphotons and multijets is estimated in sideband [2] with the data-driven method as described in Section 7.3.

The simulation under MC15c configuration is used in the analysis. The samples are generated with the consideration of multiple interactions per bunch crossing by introducing pileup noise at the stage of digitization. MC15c configuration incorporates the pileup condition that is an average of the actual pileup condition in 2015 data and an estimation for 2016 data.

3.2.1 MC samples for signals

Signal samples are generated with MadGraph5_aMC@NLO [15]. For both non-resonant and resonant productions, the event generation is performed using a next-to-leading-order SM Higgs pair model developed by the Cosmology, Particle Physics and Phenomenology (CP3) theory group [16]. Events are generated with a Higgs Effective Field Theory (HEFT) using aMC@NLO method [17] and are reweighted to take into account top quark mass dependence. The top mass can become an important effect [18], particularly for the non-resonant case. The shower is implemented by Herwig++ [19] with UEEE5 underlying-event tune [20], and the PDF set CTEQ6L1 [21] is used. The heavy scalar, H, is assumed to have a narrow width. Technically its decay width is set to 10 MeV in the event generation for the following masses: 260 GeV, 300 GeV, 400 GeV, 500 GeV, 750 GeV, 1 TeV, 1.5 TeV, 2 TeV, 2.5 TeV, and 3 TeV. The generator level filter *ParentChildFilter* implements the selection of these decay products. Details on the signal samples are listed in Table 1. All signal samples are produced with the ATLAS fast simulation framework (AF2).

3.2.2 MC samples for SM single Higgs backgrounds

Simulated samples for SM single Higgs background are produced to investigate the components of this background in $m_{\gamma\gamma}$ and to estimate their contributions. The SM single Higgs background considered here is assumed to be produced via five production modes: gluon-gluon fusion (ggh), vector boson fusion, (VBF), Higgsstrahlung (Wh and Zh) and Higgs associated production with a pair of top quarks ($t\bar{t}h$), where h is the light (SM-like) 125 GeV Higgs boson. These samples are simulated using the full ATLAS simulation and reconstruction chain. The mass of the SM Higgs boson is set to 125 GeV. More details on generator, parton shower and simulation tags are listed in Table 2.

The cross sections at $\sqrt{s}$ = 13 TeV corresponding to each production mode are listed in Table 3. In the analysis, these cross sections will be multiplied by the $h \to \gamma\gamma$ branching ratio of 0.00228, since all simulated samples are produced with SM Higgs decaying into photon pairs.

[1] Good Run Lists are data15_13TeV.periodAllYear_DetStatus-v79-repro20-02_DQDefects-00-02-02_PHYS_StandardGRL_All_Good_25ns.xml for 2015 data and data16_13TeV.periodAllYear_DetStatus-v82-pro20-12_DQDefects-00-02-04_PHYS_StandardGRL_All_Good_25ns.xml for 2016 data

[2] The sideband is defined as $m_{\gamma\gamma} \in [105, 160]$ GeV excluding the Higgs mass window as defined in Section 5.

DSID	Processes	Generators, tunes and PDFs	Tags
342621	non-resonant	MadGraph + Herwigpp UEEE5 CTEQ6L1	$e4419\_a766\_a821\_r7676\_p2691$
343756	$X \to hh$, 260 GeV	MadGraph + Herwigpp UEEE5 CTEQ6L1	$e5153\_a766\_a821\_r7676\_p2691$
343758	$X \to hh$, 300 GeV	MadGraph + Herwigpp UEEE5 CTEQ6L1	$e5153\_a766\_a821\_r7676\_p2691$
343761	$X \to hh$, 400 GeV	MadGraph + Herwigpp UEEE5 CTEQ6L1	$e5153\_a766\_a821\_r7676\_p2691$
343763	$X \to hh$, 500 GeV	MadGraph + Herwigpp UEEE5 CTEQ6L1	$e5153\_a766\_a821\_r7676\_p2691$
343818	$X \to hh$, 750 GeV	MadGraph + Herwigpp UEEE5 CTEQ6L1	$e5153\_a766\_a821\_r7676\_p2691$
343819	$X \to hh$, 1000 GeV	MadGraph + Herwigpp UEEE5 CTEQ6L1	$e5153\_a766\_a821\_r7676\_p2691$
343820	$X \to hh$, 1500 GeV	MadGraph + Herwigpp UEEE5 CTEQ6L1	$e5153\_a766\_a821\_r7676\_p2691$
343821	$X \to hh$, 2000 GeV	MadGraph + Herwigpp UEEE5 CTEQ6L1	$e5153\_a766\_a821\_r7676\_p2691$
343822	$X \to hh$, 2500 GeV	MadGraph + Herwigpp UEEE5 CTEQ6L1	$e5153\_a766\_a821\_r7676\_p2691$
343823	$X \to hh$, 3000 GeV	MadGraph + Herwigpp UEEE5 CTEQ6L1	$e5153\_a766\_a821\_r7676\_p2691$

Table 1: Simulated signal samples

DSID	Processes	Generators, tunes and PDFs	Tags
341000	ggh	Powheg+Pythia8 AZNLO CTEQ6L1	$e3806\_s2608\_r7772\_r7676\_p2669$
341001	VBF	Powheg+Pythia8 AZNLO CTEQ6L1	$e3806\_s2608\_r7772\_r7676\_p2669$
341067	Wh	Pythia8 A14 NNPDF2.3LO	$e3796\_s2608\_s2183\_r7772\_r7676\_p2669$
341068	Zh	Pythia8 A14 NNPDF2.3LO	$e3796\_s2608\_s2183\_r7772\_r7676\_p2669$
341069	$t\bar{t}h$	Pythia8 A14 NNPDF2.3LO	$e3796\_s2608\_s2183\_r7772\_r7676\_p2669$

Table 2: Simulated SM single Higgs background samples.

production	cross sections
ggh	48.52 pb
VBF	3.779 pb
Wh	1.369 pb
Zh	0.8824 pb
$t\bar{t}h$	0.5065 pb
$gg \to hh$	33.41 fb

Table 3: Cross sections for SM single Higgs processes at $\sqrt{s} = 13$ TeV with $m_h = 125.09$ GeV and the SM Higgs pair productions, $gg \to hh$.

4 Object definition

The object definition is similar to what is used by the HGam group. The analysis framework of $hh \to \gamma\gamma WW^*$ is based on the HGamAnalysisFramework that is centrally developed by HGam group. The tag of the framework is HGamAnalysisFramework-00-02-55-11 which is used to produce official MxAOD samples of version h013a.

4.1 Photons

- The E_{T} of leading (sub-leading) photon is required to be larger than 25 GeV.
- The $|\eta|$ of photon is considered up to 2.37, vetoing the crack region $1.37 < |\eta| < 1.52$.
- Tight photons are required, as is the default in HGam group. The photon identification algorithm is based on the lateral and longitudinal energy profiles of the shower measured in the electromagnetic calorimeter.
- The isolation working point FixedCutLoose is used. It is one of the recommended points from the isolation forum. Photons are required to pass both calorimeter-based and track-based isolation requirements.
- Photons are passed through the e/γ ambiguity tool, as is the default in the HGam group. The ambiguity tool is developed to discriminate photons and electrons that can otherwise have overlapping selections. In particular, converted photons from electrons in the silicon can lead to large e/γ fake rate. The ambiguity tool makes requirements on the number of silicon hits and the conversion rates to keep this rate under control without significant loss of signal efficiency.

4.2 Jets

- The anti-k_t algorithm [22] with the size parameter of $R = 0.4$ is used to reconstruct jets from topological clusters in the calorimeters that are calibrated to the EM scale.
- Jets undergo an energy calibration.
- Jets are required to have $p_{\mathrm{T}} > 25$ GeV and $|\eta| < 2.5$.
- Jets from pileup are suppressed by applying a JVT (Jet Vertex Tagger) cut. The jet is rejected if JVT< 0.59 for $p_{\mathrm{T}} < 60$ GeV and $|\eta| < 2.4$.
- Events with a jet passing the LooseBad cut are rejected. The LooseBad jet quality requirement is designed to reject fake jets caused by detector readout problems and non-collision backgrounds.

4.3 Electrons

Electrons are reconstructed from energy clusters in the EM calorimeter matched with tracks reconstructed in the inner detector.

- E_{T} is required to be larger than 10 GeV.
- $|\eta|$ is required to be less than 2.47 vetoing the transition region with $1.37 < |\eta| < 1.52$.
- The $|d_0|$ significance ($d_0/\sigma(d_0)$) with respect to the primary vertex in the event is required to be less than 5.

- The $|z_0|$ with respect to the primary vertex in the event is required to be less than 0.5 mm.
- Identification: Medium quality electrons are used.
- Isolation: Loose electrons are used.

4.4 Muons

Muons are reconstructed from tracks in the inner detector and the muon spectrometer.

- p_T is required to be larger than 10 GeV.
- $|\eta|$ is required to be less than 2.7.
- The $|d_0|$ significance with respect to the primary vertex in the event is required to be less than 3.
- The $|z_0|$ with respect to the primary vertex in the event is required to be less than 0.5 mm.
- Identification: Medium quality muons are used.
- Isolation: GradientLoose is used.

4.5 Overlap removal

Since the collections of objects are reconstructed using different algorithms in parallel (i.e. there is no check to prevent a single cluster or track from being included in the reconstruction of two different object) it is necessary to implement a set of rules to remove objects nearby each other to avoid double counting. The rules are implemented sequentially as defined below:

- The two leading photons are always kept.
- Electrons with $\Delta R(e, \gamma) < 0.4$ are removed.
- Jets with $\Delta R(jet, \gamma) < 0.4$ are removed.
- Jets with $\Delta R(jet, e) < 0.2$ are removed.
- Muons with $\Delta R(\mu, \gamma) < 0.4$ or $\Delta R(\mu, jet) < 0.4$ are removed
- Electrons with $\Delta R(e, jet) < 0.4$ are removed.

5 Event selection

The event selection procedure identifies two photons and then applies requirements on the multiplicities of jets in order to increase the signal purity and background rejection for events with multi-jets. This analysis selects events with a boosted topology as well as events with a resolved topology. The event selection for the analysis starts with the full di-photon selection from the $h \to \gamma\gamma$ analysis in RUN II to select two high p_{T} isolated photons.

- **Trigger**: Events are required to pass at least one of the following diphoton triggers, using a logical OR: `HLT_g35_loose_g25_loose` or `HLT_g35_medium_g25_medium` or `HLT_2g50_loose` or `HLT_2g20_tight`.
- **Good Run List and Detector Quality**: Events must belong to the luminosity blocks specified in the Good Run Lists:
  - data15_13TeV.periodAllYear_DetStatus-v79-repro20-02_DQDefects-00-02-02_PHYS_StandardGRL_All_Good_25ns.xml for 2015 data
  - data16_13TeV.periodAllYear_DetStatus-v82-pro20-12_DQDefects-00-02-04_PHYS_StandardGRL_All_Good_25ns.xml for 2016 data

  These GRLs reject events with data integrity errors in the calorimeters and incomplete events where some detector information is missing are rejected, as well as events which are corrupted due to power supply trips in the tile calorimeter.
- **Primary Vertex**: The primary vertex is selected using the neural network algorithm from HGam group. The photons' four momenta, JVT and track isolation are corrected with respect to this origin, and the mass of the diphoton system is accordingly recalculated.
- **2 loose photons**: At least two loose photons with $E_{\mathrm{T}} > 25$ GeV and within the detector acceptance are selected.
- The other cuts on photons involving **Identification (tight ID), Isolation, Rel.Pt cuts**. The relative p_{T} cut requires the p_{T} of leading (sub-leading) photon to be larger than 0.35(0.25) of diphoton invariant mass. The diphoton invariant mass is required to be within the range $m_{\gamma\gamma} \in [105, 160]$ GeV.
- **Higgs mass window**: $|m_{\gamma\gamma} - m_h| < 2\sigma_{m_{\gamma\gamma}}$ is also required where $m_h = 125.09$ GeV is the measured SM Higgs boson mass and $\sigma_{m_{\gamma\gamma}} = 1.7$ GeV is the experimental diphoton mass resolution. This selection is only used to define signal region and sideband.
- **Lepton veto**: Events are required to contain exactly zero electrons or muons.
- ***b*-veto**: In order to suppress backgrounds with top quarks and ensure orthogonality to other *hh* searches ($bb\gamma\gamma$, $bbbb$, $bb\tau\tau$, etc.), the event is rejected if there are any *b*-tagged jets. The *b*-tagger is MV2c10 with a *b*-tagging efficiency of 70%.
- **jet multiplity**: Considering the jet p_{T} at truth level, the two categories are defined by exact 3 jets or at least 4 jets to enlarge signal efficiency.

The efficiencies of common event selection are listed in Table 4. These efficiencies are derived for signals from simulated samples. After the selection of the two photons, the signal efficiencies range from 36.5% to 42.4%, while after the additional selection on the jets and the leptons on the di-photon, the signal efficiencies range from 12.6% to 28.3%, for a resonant mass from 260 and 500 GeV.

	SM	Resonant hh			
	Higgs pair	260 GeV	300 GeV	400 GeV	500 GeV
All Events	100.0%	100.0%	100.0%	100.0%	100.0%
Duplicate	100.0%	100.0%	100.0%	100.0%	100.0%
GRL	100.0%	100.0%	100.0%	100.0%	100.0%
Pass Trigger	71.6%	67.3%	67.7%	69.7%	72.8%
2 loose photons	59.1%	56.3%	55.9%	57.3%	59.9%
Tight ID	49.4%	46.3%	45.6%	47.5%	50.2%
Isolation	44.7%	39.2%	39.1%	42.6%	45.9%
Rel.Pt cuts	41.2%	36.6%	35.5%	38.7%	42.6%
$105 < m_{\gamma\gamma} < 160$ GeV	41.0%	36.5%	35.4%	38.6%	42.4%
lepton veto	40.9%	35.1%	35.3%	38.5%	42.3%
B-veto	38.2%	33.6%	33.6%	36.1%	39.2%
jet multiplicity	25.6%	12.6%	16.1%	23.2%	28.3%

Table 4: Efficiencies for the common event selection criteria

6 Selection optimization

The event selection is further optimized to select the WWyy full hardronic events. In the optimization, the signal cross section $\sigma(pp \rightarrow hh)$ is assumed to be 1 pb. The signal modeling and the estimation of the SM Higgs background are both from MC. Data sideband $|m_{\gamma\gamma} - 125.09| > 3.4GeV$ is used to model the continuum background. As the signal jets from W boson are very soft, one of the signal jets is likely to fail the jet pT cut. Therefore the events are split into exact 3 jet category and at least 4 jet category to cover this. The pT of signal jets at truth level can be found in Figure 1.

The general selection optimization is as following. First, define a mass window of diphoton containing 85 % signal events for resonant search. Second, a scan on $pT_{\gamma\gamma}$ is performed to improve the significance since the SM Higgs will be boosted in di-Higgs event. The significance is calculated by Eq 1, where the yields of BSM signal and SM Higgs are estimated from MC and the continuum background yield is estimated from an exponential fit on data sideband.

$$\sigma_{signal} = \sqrt{2 \times \left\{ (N_{signal} + N_{SM\ Higgs} + N_{continuum}) \times ln(1 + \frac{N_{signal}}{N_{SM\ Higgs} + N_{continuum}}) - N_{signal} \right\}} \quad (1)$$

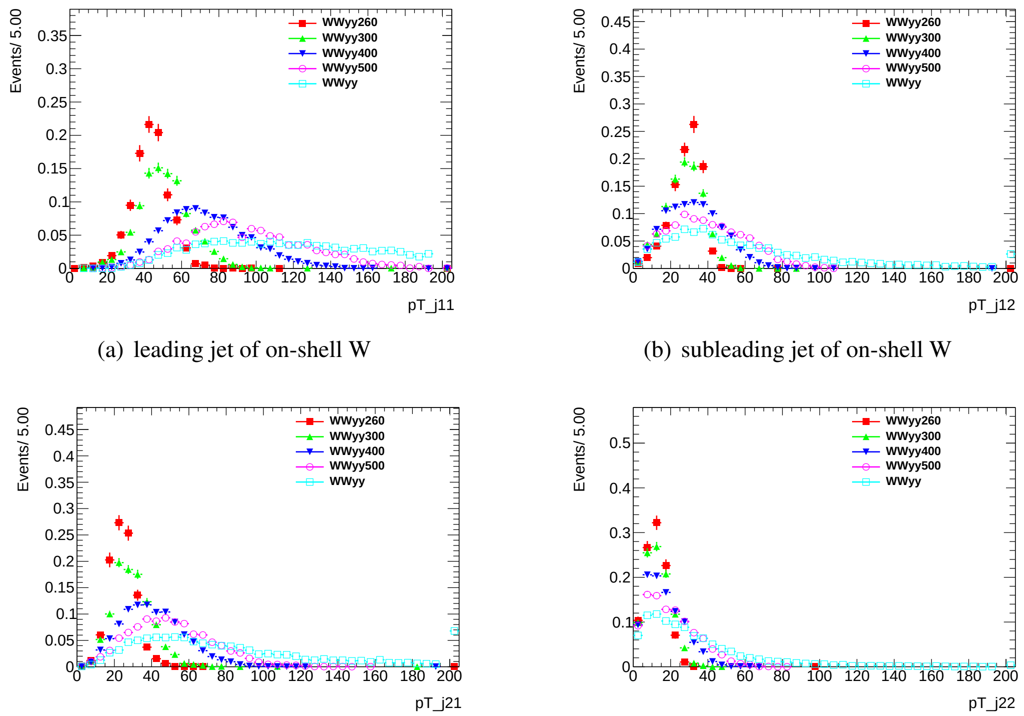

(a) leading jet of on-shell W

(b) subleading jet of on-shell W

(c) leading jet of off-shell W

(d) leading jet of off-shell W

Figure 1: pT of four signal jets at truth level

6.1 Baseline strategy

The first strategy used in this analysis simply chooses the 85% signal efficiency diphoton mass window for 3 jet and 4 jet categories and scans the pT of the diphoton to maximize the signal significance as mentioned above. This is done for different resonant mass from 260 GeV to 500 GeV. The invariant mass distribution of diphoton for 3 jet and 4 jet categories is shown in Figure 2. And Figure 3 shows the defined mass windows that contain 85 % of signal yields. The distribution of $pT_{\gamma\gamma}$ is shown in Figure 4. The scan on $pT_{\gamma\gamma}$ as a function of significance is shown on Figure 5, Figure 6, Figure 7, Figure 8, Figure 9 for resonance masses from 260 GeV to 500 GeV, respectively. Table 5 summarizes the final optimization cuts and results. More details about the additional optimization can be seen in Appendix A.

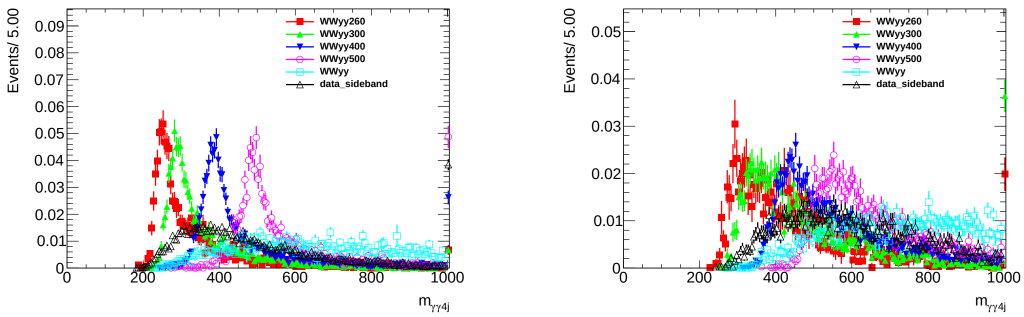

(a) 3 jet category (b) 4 jet category

Figure 2: invariant mass of $\gamma\gamma + 3\ or\ 4\, jets$

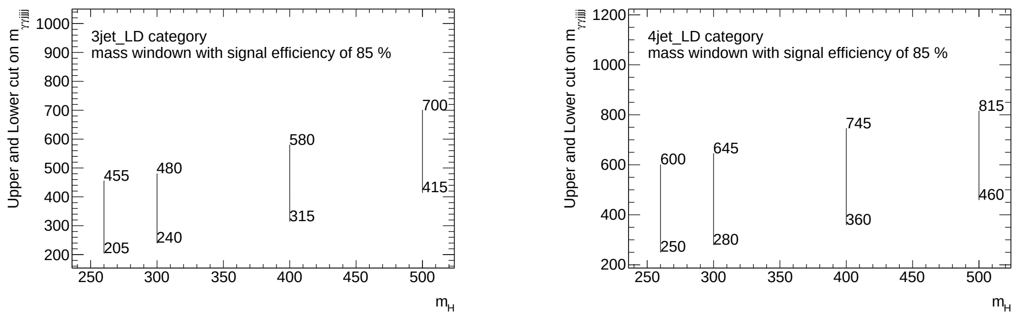

(a) 3 jet category (b) 4 jet category

Figure 3: mass window of $m_{\gamma\gamma 4(3)j}$ containing 85 % of signal events

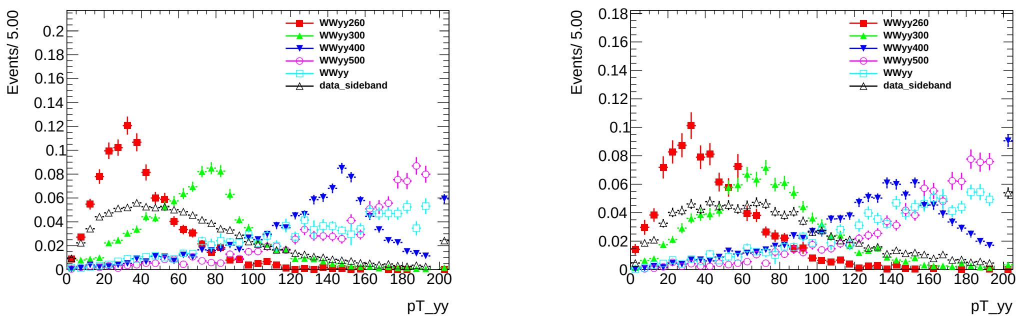

(a) 3 jet category (b) 4 jet category

Figure 4: $pT_{\gamma\gamma}$ distribution in 3 jet and 4 jet category

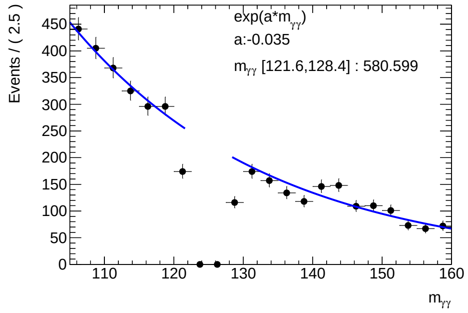

(a) data sideband fit of 3 jet category

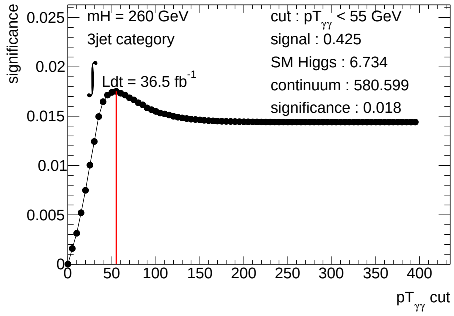

(b) data sideband fit of 4 jet category

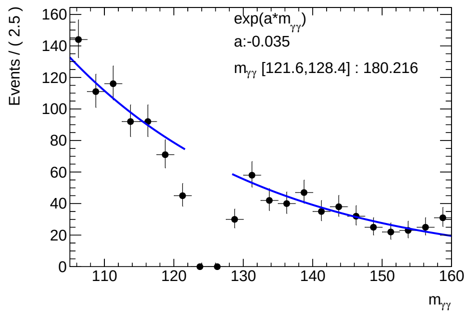

(c) cut scan of 3 jet category

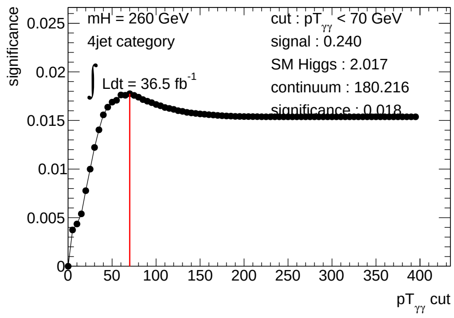

(d) cut scan of 4 jet category

Figure 5: scan the $pT_{\gamma\gamma}$ cut and plot the data sideband fit for m_H = 260 GeV.

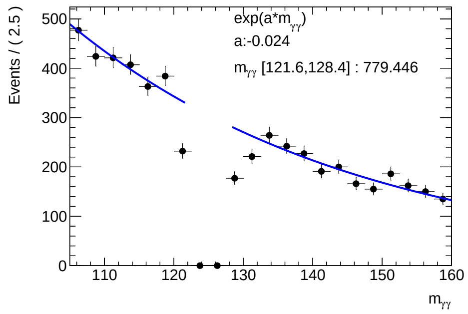

(a) data sideband fit of 3 jet category

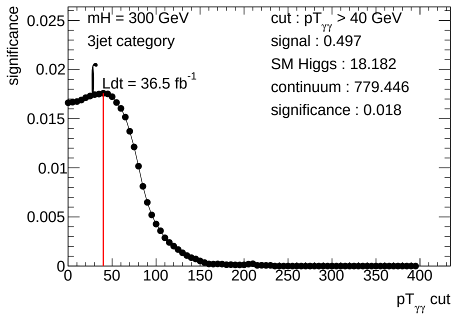

(b) data sideband fit of 4 jet category

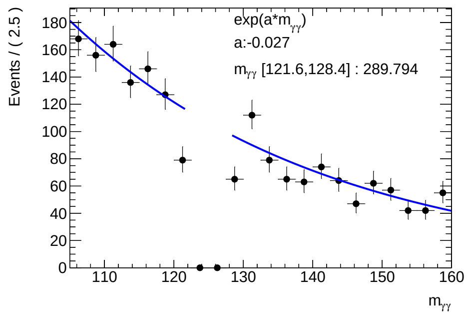

(c) cut scan of 3 jet category

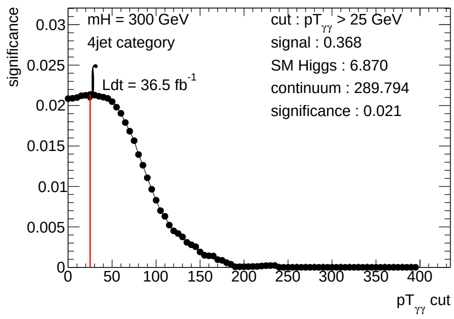

(d) cut scan of 4 jet category

Figure 6: scan the $pT_{\gamma\gamma}$ cut and plot the data sideband fit for m_H = 300 GeV.

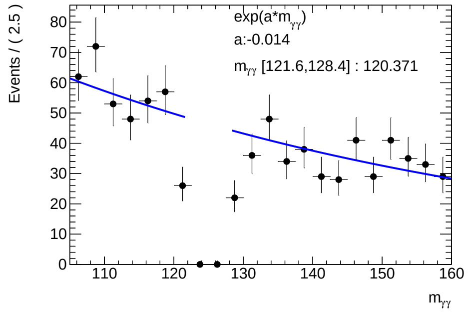

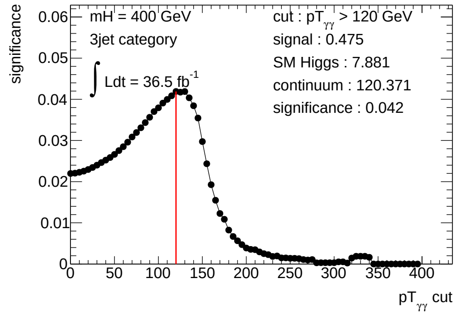

(a) data sideband fit of 3 jet category

(b) data sideband fit of 4 jet category

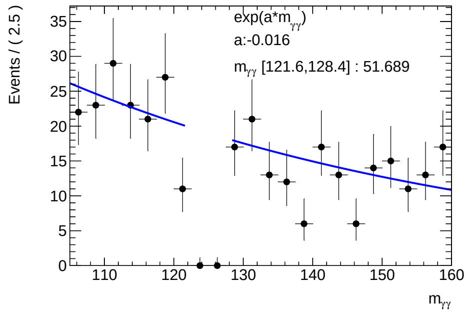

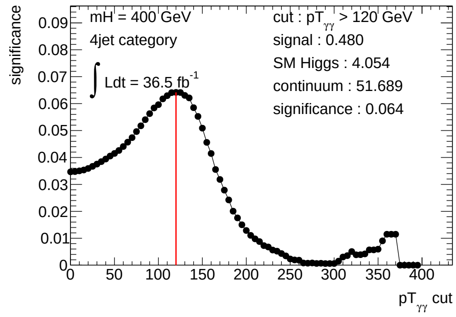

(c) cut scan of 3 jet category

(d) cut scan of 4 jet category

Figure 7: scan the $pT_{\gamma\gamma}$ cut and plot the data sideband fit for $m_H = 400$ GeV.

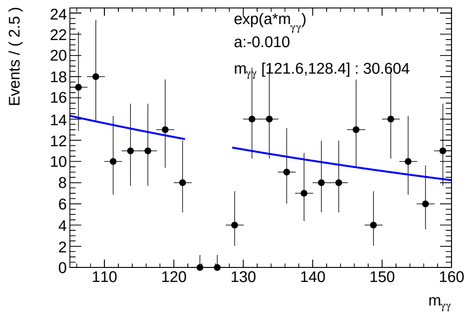

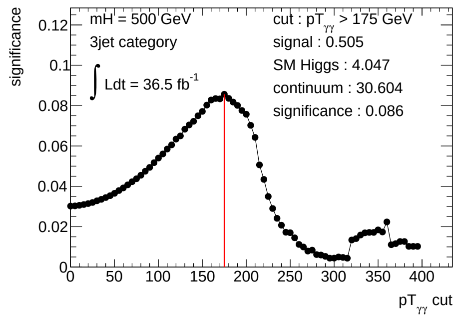

(a) data sideband fit of 3 jet category

(b) data sideband fit of 4 jet category

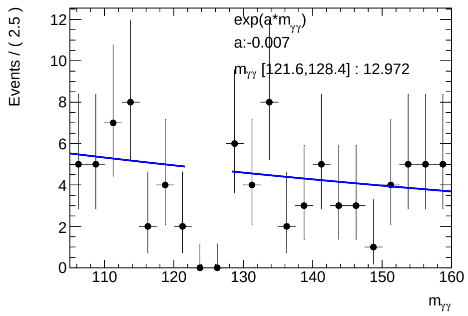

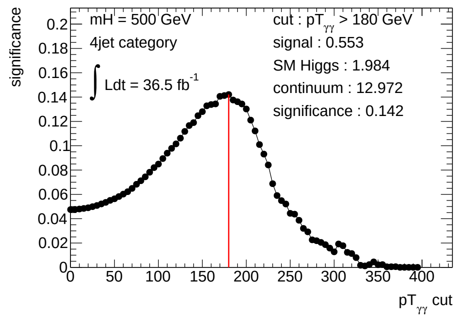

(c) cut scan of 3 jet category

(d) cut scan of 4 jet category

Figure 8: scan the $pT_{\gamma\gamma}$ cut and plot the data sideband fit for $m_H = 500$ GeV.

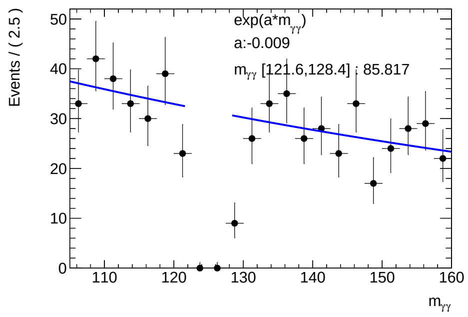

(a) data sideband fit of 3 jet category

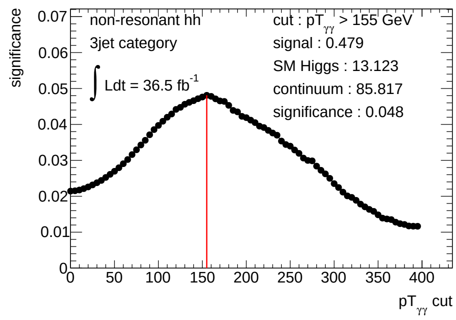

(b) data sideband fit of 4 jet category

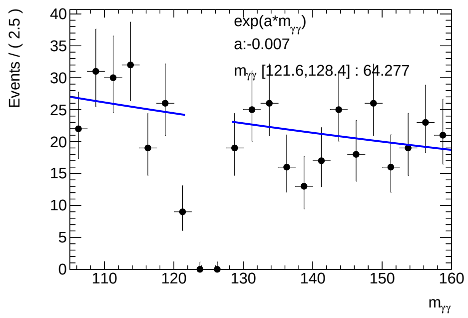

(c) cut scan of 3 jet category

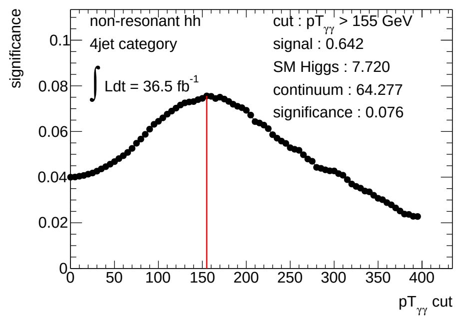

(d) cut scan of 4 jet category

Figure 9: scan the $pT_{\gamma\gamma}$ cut and plot the data sideband fit for non-resonant.

	non-res		260 GeV		300 GeV		400 GeV		500 GeV	
mass window [GeV]	-	-	[205, 455]	[250, 600]	[240, 480]	[280, 645]	[315, 580]	[360, 745]	[415, 700]	[460, 815]
$pT_{\gamma\gamma}[GeV]$ cut	> 155	> 155	< 55	< 70	> 40	> 25	> 120	> 120	> 175	> 180
signal yield	0.48	0.64	0.43	0.24	0.50	0.37	0.48	0.48	0.51	0.55
SM Higgs	13.12	7.72	6.73	2.02	18.18	6.87	7.88	4.05	4.05	1.98
continuum	85.82	64.28	580	180	779	289	120	51	31	13
significance	0.048	0.076	0.018	0.018	0.018	0.021	0.042	0.064	0.086	0.142
combined significance	0.090		0.025		0.028		0.077		0.166	

Table 5: summary of selection, yield and significance

7 Signal and background estimations

7.1 Signal modeling

Similar to $h \to \gamma\gamma$ analysis, the signal shape of this analysis can be modeled by Double-Sided Crystal-ball(DSCB) function of Crystal-ball plus Gaussian function(CBGA). Figure 10 show the fit on $m_{\gamma\gamma}$. The difference of these two functions is the high-mass tail. From the fit quality, Double-Sided Crystal-ball describes the shape better.

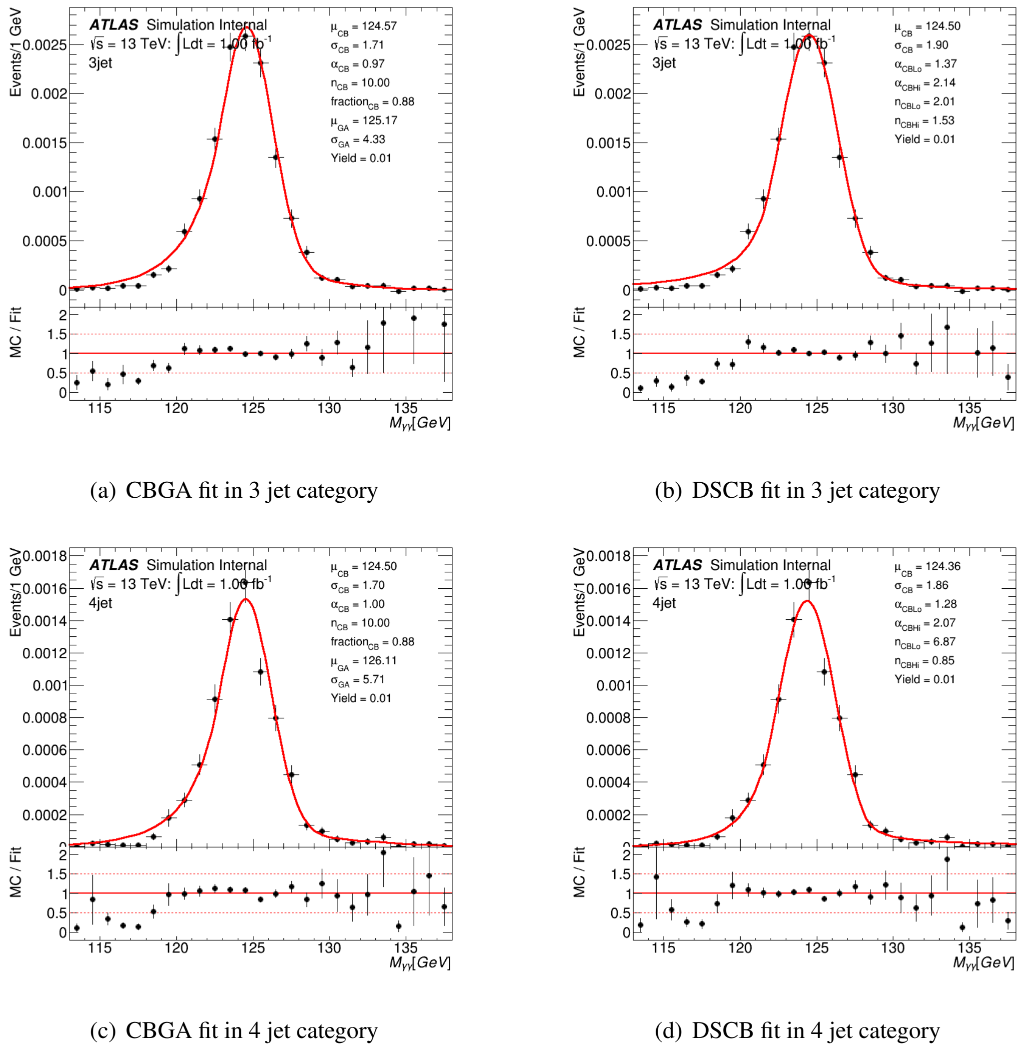

(a) CBGA fit in 3 jet category

(b) DSCB fit in 3 jet category

(c) CBGA fit in 4 jet category

(d) DSCB fit in 4 jet category

Figure 10: CBGA and DSCB fit in $m_H = 260$ GeV

7.2 Simulation of Higgs background processes

Standard Model production of a single Higgs boson with the $h \to \gamma\gamma$ decay mode are estimated using Monte Carlo simulation. Other decay modes are not considered because they do not contribute to the Higgs-mass peak in the $m_{\gamma\gamma}$ spectrum. The processes considered are gluon-gluon fusion, vector boson fusion, Higgsstrahlung, and Higgs production :in association with $t\bar{t}$. In gluon-gluon fusion events, all jets are the result of ISR. In vector boson fusion events, ISR and FSR are responsible for the extra jets

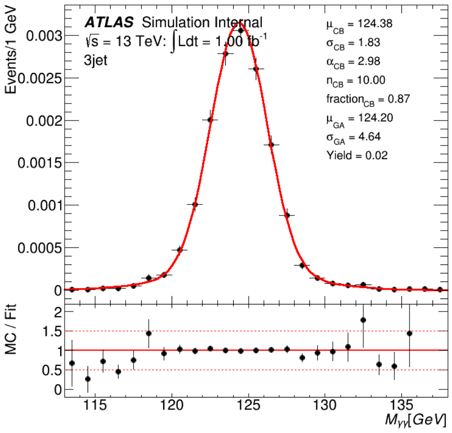

(a) CBGA fit in 3 jet category

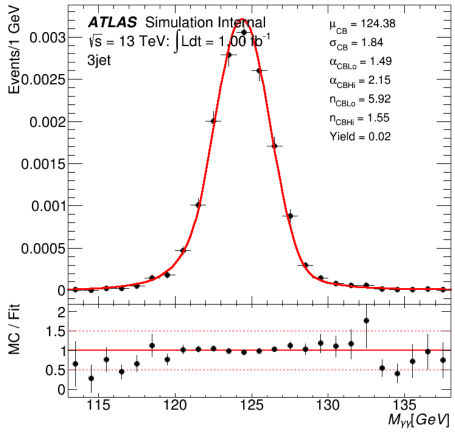

(b) DSCB fit in 3 jet category

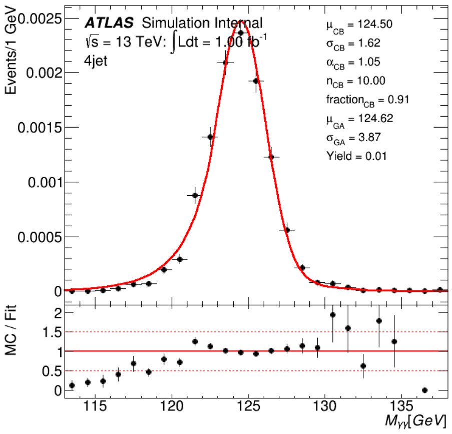

(c) CBGA fit in 4 jet category

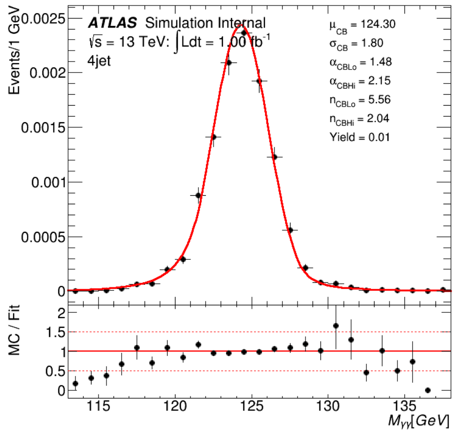

(d) DSCB fit in 4 jet category

Figure 11: CBGA and DSCB fit in m_H = 300 GeV

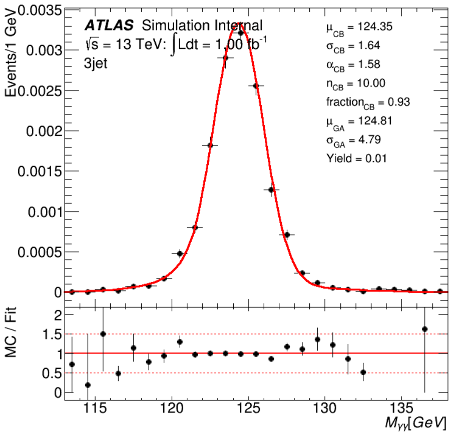

(a) CBGA fit in 3 jet category

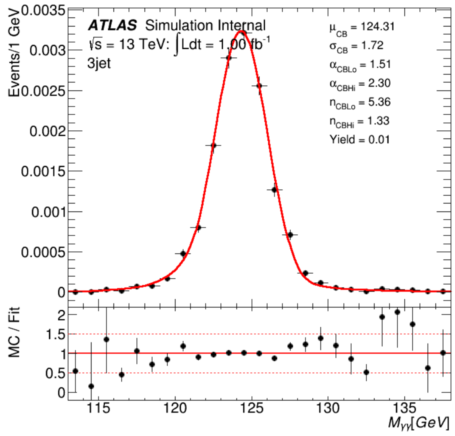

(b) DSCB fit in 3 jet category

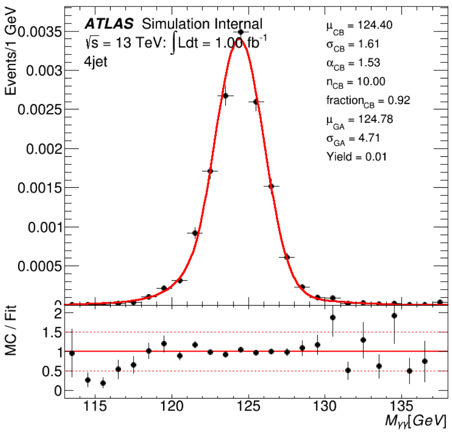

(c) CBGA fit in 4 jet category

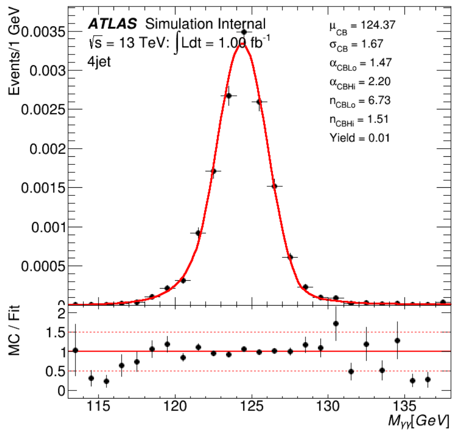

(d) DSCB fit in 4 jet category

Figure 12: CBGA and DSCB fit in m_H = 400 GeV

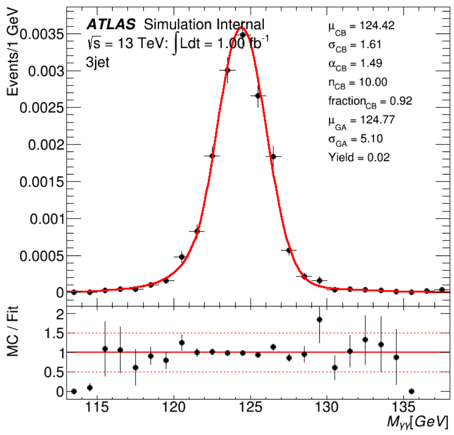

(a) CBGA fit in 3 jet category

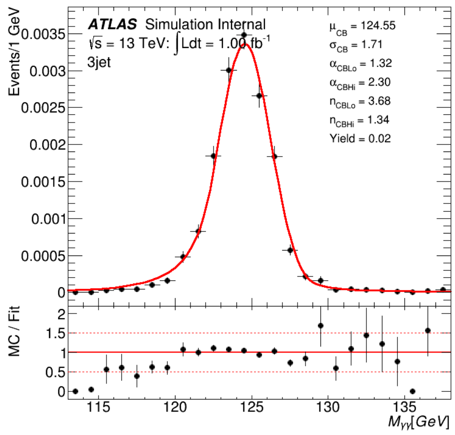

(b) DSCB fit in 3 jet category

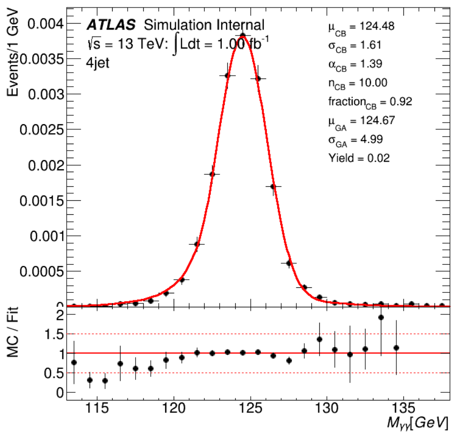

(c) CBGA fit in 4 jet category

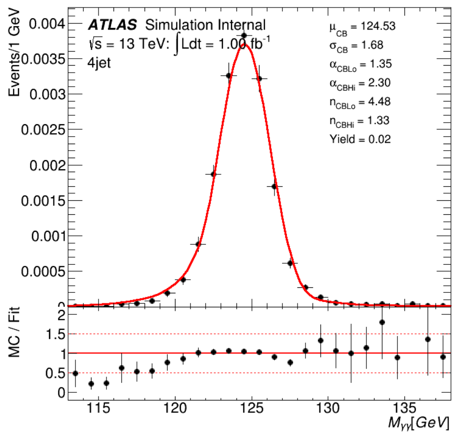

(d) DSCB fit in 4 jet category

Figure 13: CBGA and DSCB fit in m_H = 500 GeV

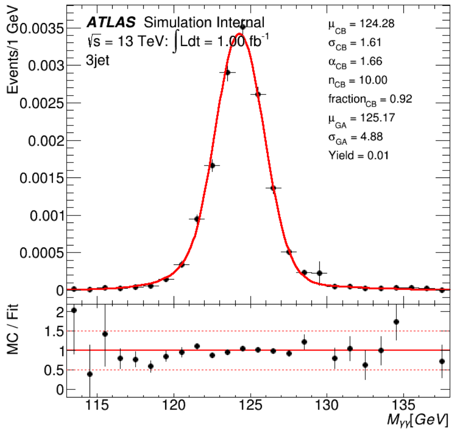

(a) CBGA fit in 3 jet category

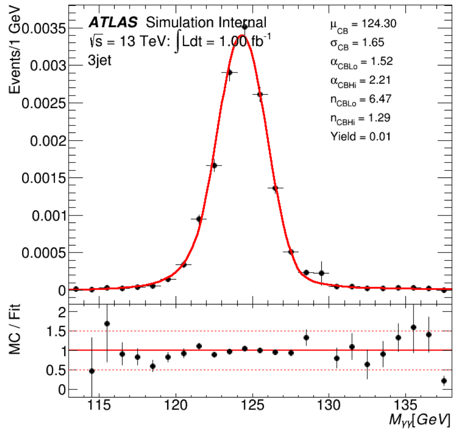

(b) DSCB fit in 3 jet category

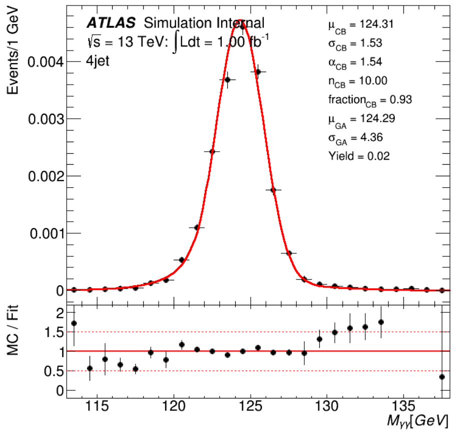

(c) CBGA fit in 4 jet category

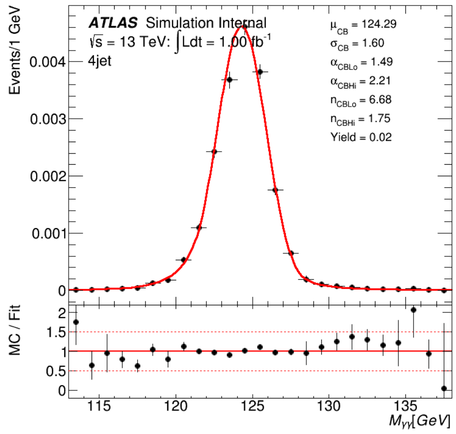

(d) DSCB fit in 4 jet category

Figure 14: CBGA and DSCB fit in non-resonant search

in addition to the forward jets from the scattered quarks in vector boson fusion and the hadronic decay products of the W- or Z-boson in Higgsstrahlung. In the case of $t\bar{t}$+h events, a sufficient number of jets are produced from the decay of the two top quarks. The $m_{\gamma\gamma}$ shape SM Higgs is also modeled by Double-Sided Crystal-ball or Crystal-ball plus Gaussian function.

Double-Sided Crystal-ball is chosen to describe the SM Higgs background. (Currently Drystal-ball plus Gaussian is implemented in the workspace)

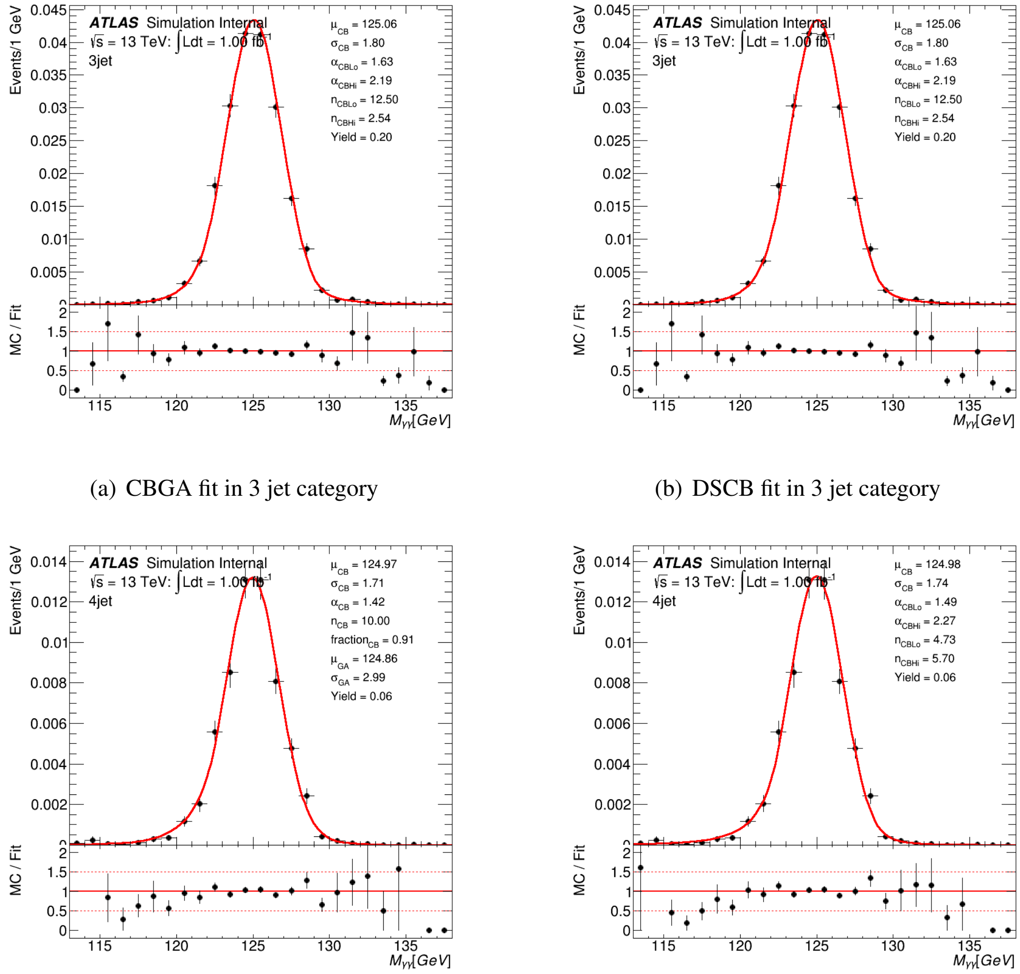

(a) CBGA fit in 3 jet category

(b) DSCB fit in 3 jet category

(c) CBGA fit in 4 jet category

(d) DSCB fit in 4 jet category

Figure 15: CBGA and DSCB fit of SM Higgs background in m_H = 260 GeV

7.3 Estimating continuum background processes

The continuum background consist of $\gamma\gamma$, $\gamma - jet$ and jet-jet events. The method of spurious signal is used to choose the optimal function to describe the continuum background shape. The principle is to perform S+B fit to large statistic background-only MC sample. The fitted yield is called spurious signal, N_{sp}. The N_{sp} must pass some requirements. It must be smaller than 10 % of the expected signal yield and 20 % of the fitted signal uncertainty. If all the candidate functions pass the criteria, the function with least degree of freedom is chosen. One sample of 100M fast simulation diphoton plus up to 3 jets is produced in HGam group and it is used in spurious signal analysis. The candidate function could be

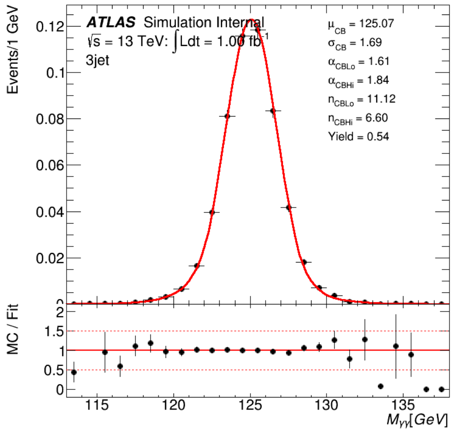

(a) CBGA fit in 3 jet category

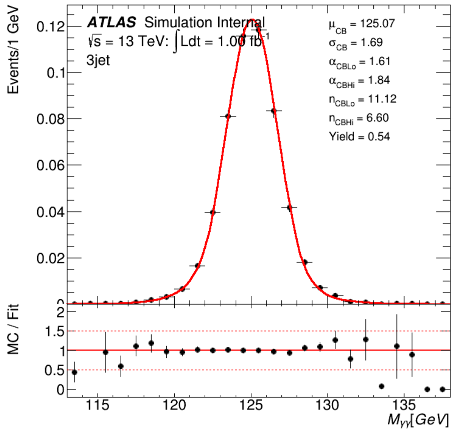

(b) DSCB fit in 3 jet category

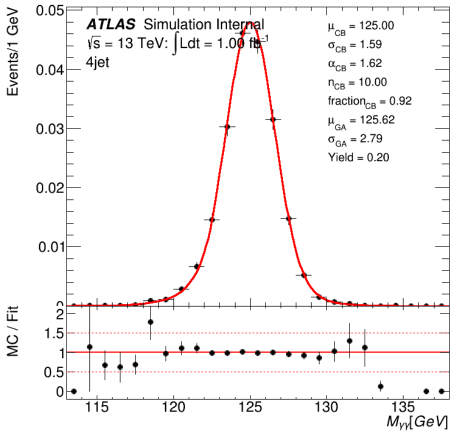

(c) CBGA fit in 4 jet category

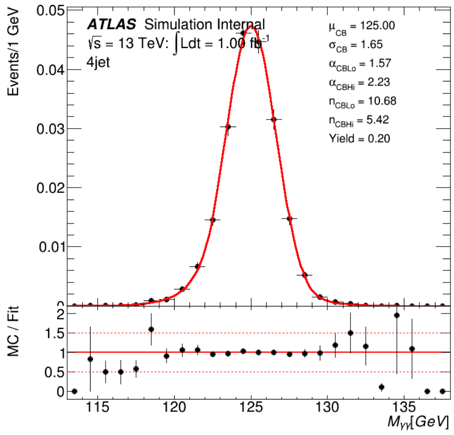

(d) DSCB fit in 4 jet category

Figure 16: CBGA and DSCB fit of SM Higgs background in $m_H = 300$ GeV

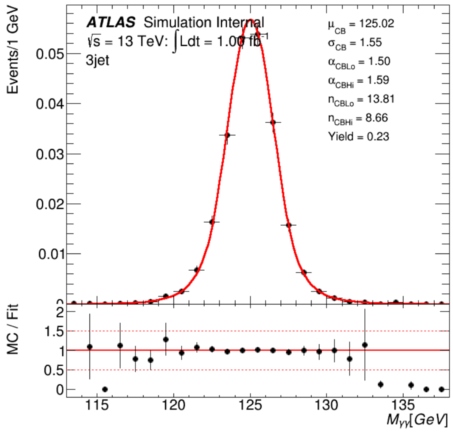

(a) CBGA fit in 3 jet category

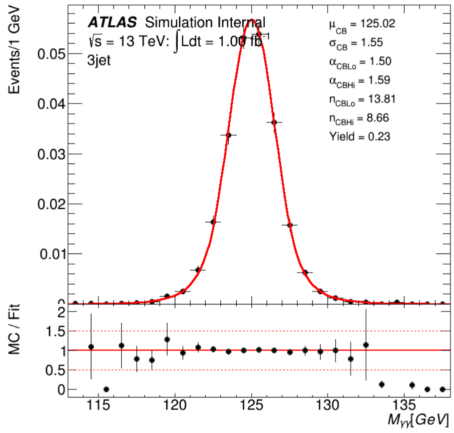

(b) DSCB fit in 3 jet category

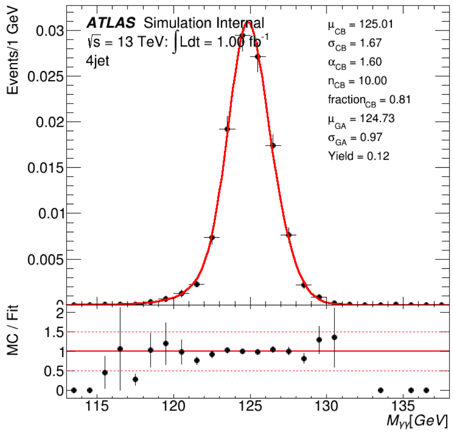

(c) CBGA fit in 4 jet category

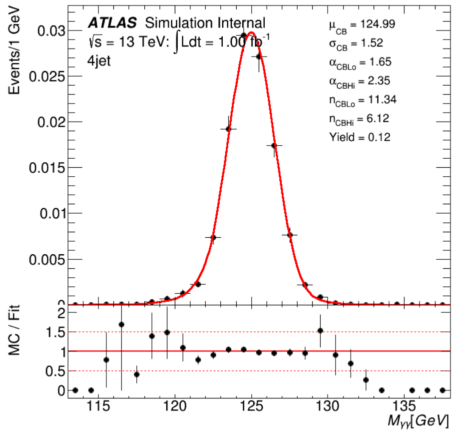

(d) DSCB fit in 4 jet category

Figure 17: CBGA and DSCB fit of SM Higgs background in $m_H = 400$ GeV

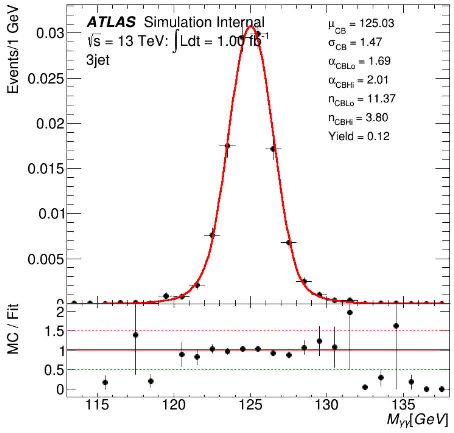

(a) CBGA fit in 3 jet category

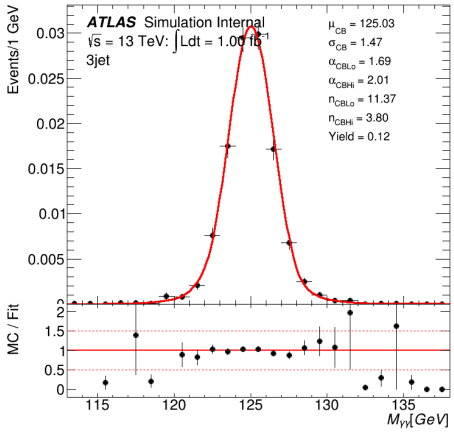

(b) DSCB fit in 3 jet category

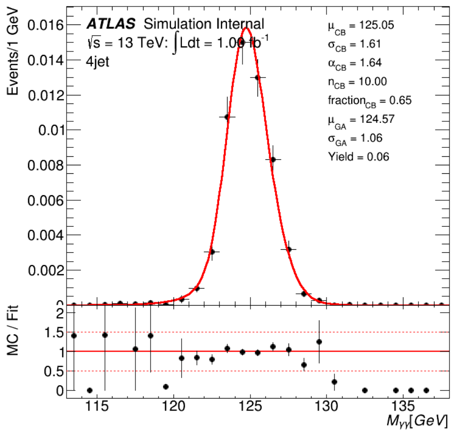

(c) CBGA fit in 4 jet category

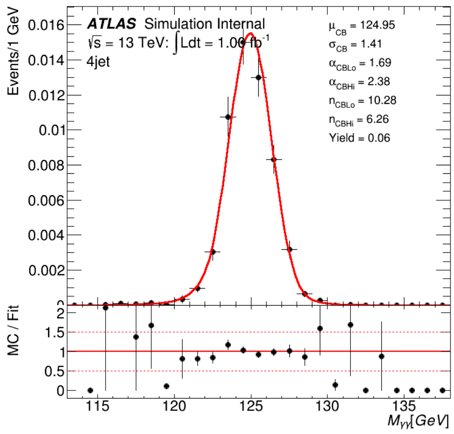

(d) DSCB fit in 4 jet category

Figure 18: CBGA and DSCB fit of SM Higgs background in m_H = 500 GeV

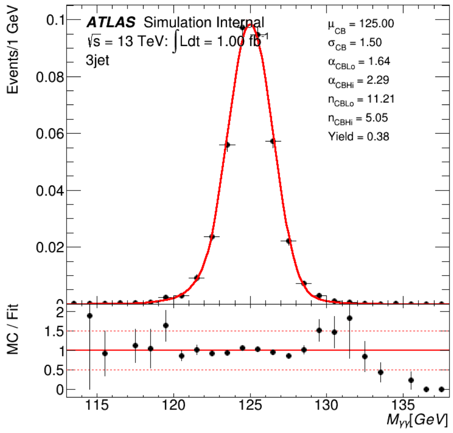

(a) CBGA fit in 3 jet category

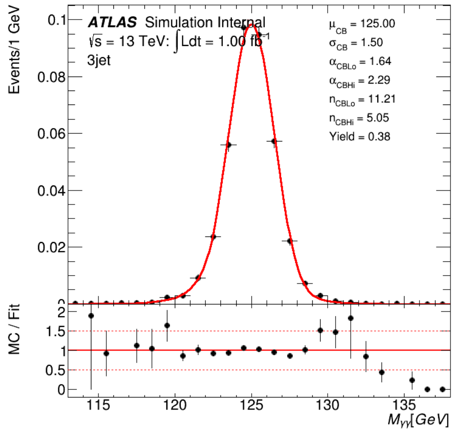

(b) DSCB fit in 3 jet category

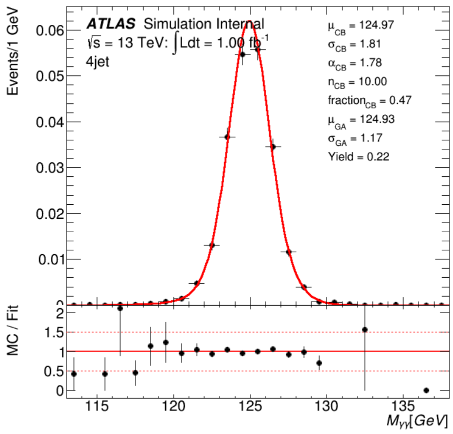

(c) CBGA fit in 4 jet category

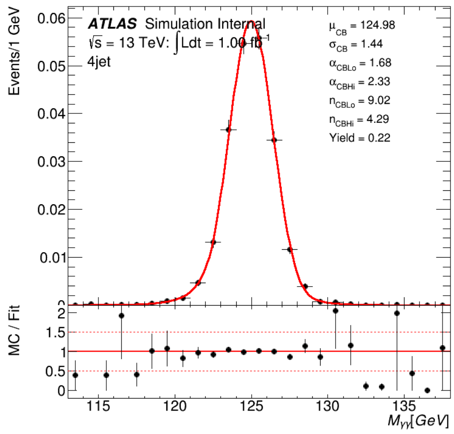

(d) DSCB fit in 4 jet category

Figure 19: CBGA and DSCB fit of SM Higgs background in non-resonant search

category	function	Max(S)	Max(S/ΔS)	Max(S/S_{ref})	status
non-res 3jet	ExpPoly2	3.221	2.443	5.929	Fail
non-res 4jet	Exponential	1.372	1.677	1.919	Fail
260 3jet	ExpPoly2	-9.178	-4.468	-18.258	Fail
260 4jet	Exponential	-3.461	-2.62	-12.097	Fail
300 3jet	ExpPoly2	-6.457	-2.128	-11.272	Fail
300 4jet	ExpPoly2	3.961	-1.873	9.349	Faiil
400 3jet	ExpPoly2	3.910	3.035	7.254	Fail
400 4jet	ExpPoly2	-1.157	-1.447	-2.133	Fail
500 3jet	ExpPoly2	-1.379	-2.01	-2.40	Fail
500 4jet	Exponential	0.849	2.07291	1.38102	Fail

Table 6: The table shows maximum spurious signal , $S/\Delta S$, S/S_{ref} of best function in [115, 135] GeV.

exponential, 2nd-exponential, Di-jet shape. Figure 24 shows the spurious signal test result. The numbers are summarized in Table 6. Due to the limited statistic after all the selection, the shape of background MC is not very smooth so fluctruation is everywhere in the spurious test and none of the candidate funcions pass the criteria. Now the input of the workspace is exponential.

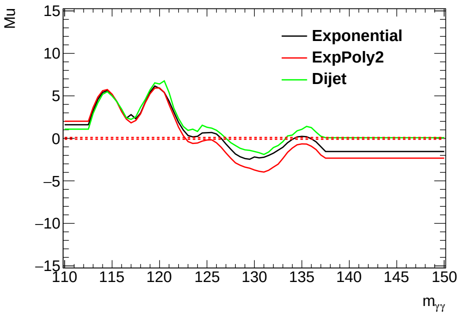

hbtp!

(a) S/S_{ref} of 3jet category for non-resonant

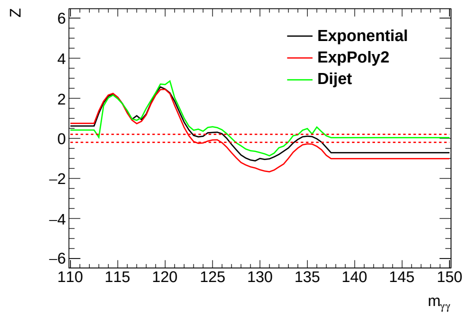

(b) $S/\Delta S$ of 3jet category for non-resonant

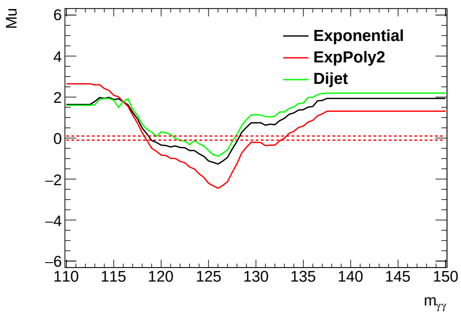

(c) S/S_{ref} of 4jet category for non-resonant

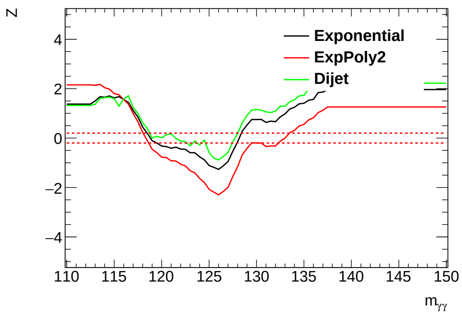

(d) $S/\Delta S$ of 4jet category for non-resonant

Figure 20:

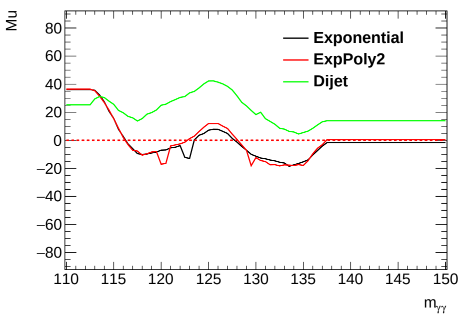

(a) S/S_{ref} of 3jet category for $m_H = 260 GeV$

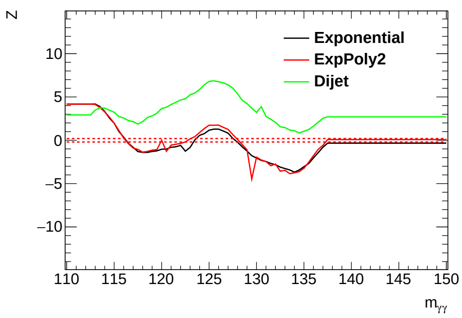

(b) $S/\Delta S$ of 3jet category for $m_H = 260 GeV$

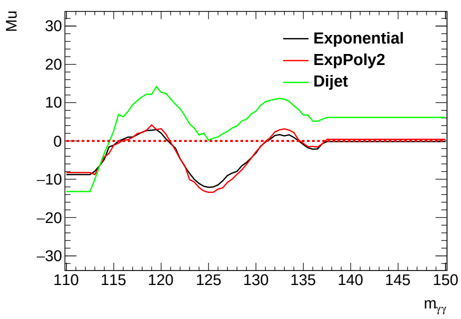

(c) S/S_{ref} of 4jet category for $m_H = 260 GeV$

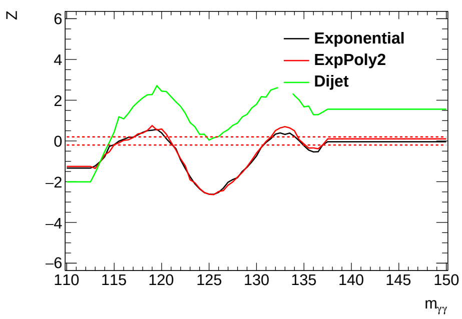

(d) $S/\Delta S$ of 4jet category for $m_H = 260 GeV$

Figure 21:

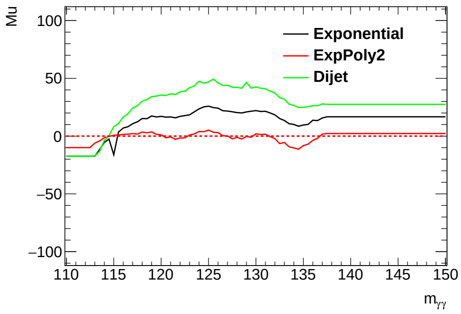

(a) S/S_{ref} of 3jet category for $m_H = 300GeV$

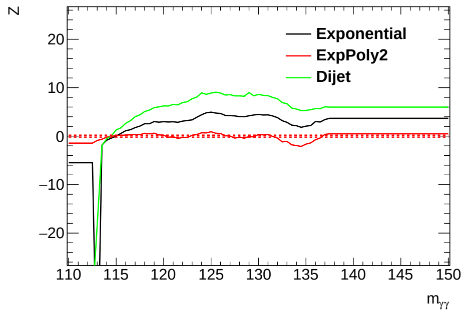

(b) $S/\Delta S$ of 3jet category for $m_H = 300GeV$

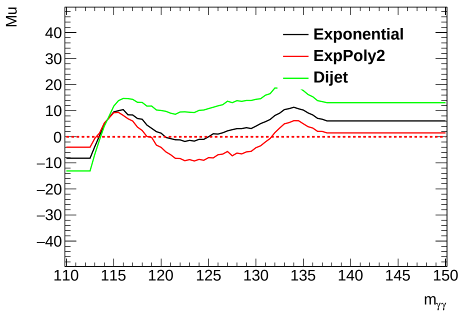

(c) S/S_{ref} of 4jet category for $m_H = 300GeV$

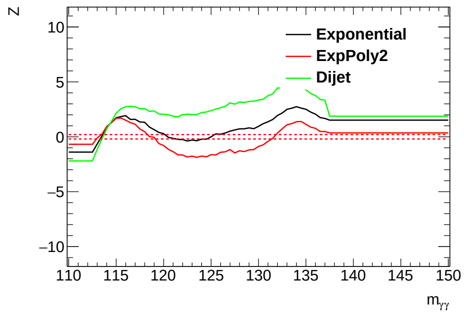

(d) $S/\Delta S$ of 4jet category for $m_H = 300GeV$

Figure 22:

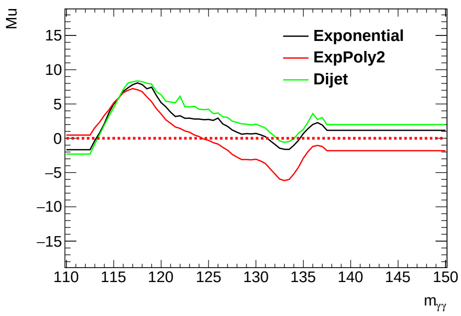

(a) S/S_{ref} of 3jet category for $m_H = 400GeV$

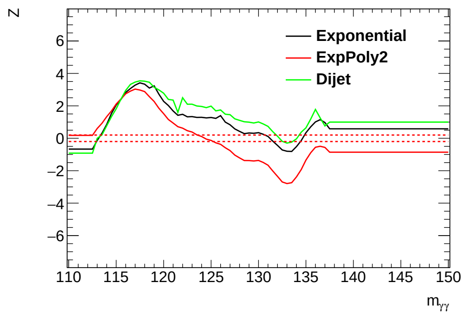

(b) $S/\Delta S$ of 3jet category for $m_H = 400GeV$

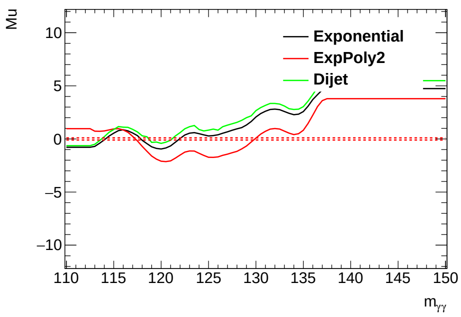

(c) S/S_{ref} of 4jet category for $m_H = 400GeV$

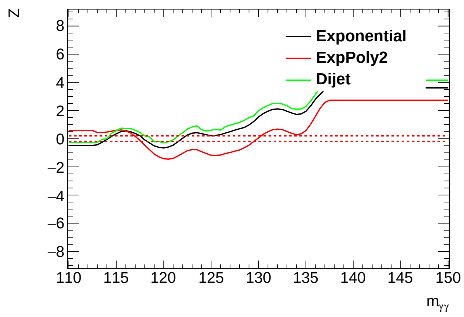

(d) $S/\Delta S$ of 4jet category for $m_H = 400GeV$

Figure 23:

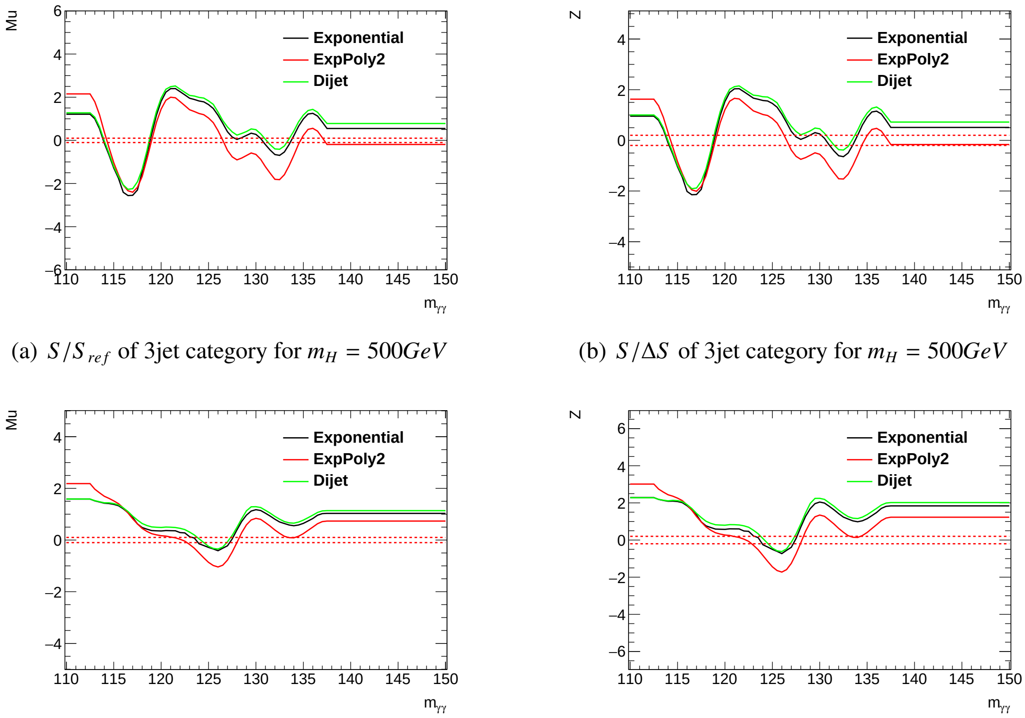

(a) S/S_{ref} of 3jet category for $m_H = 500GeV$

(b) $S/\Delta S$ of 3jet category for $m_H = 500GeV$

(c) S/S_{ref} of 3jet category for $m_H = 500GeV$

(d) $S/\Delta S$ of 3jet category for $m_H = 500GeV$

Figure 24: $S/\Delta S$ and S/S_{ref} in each category

8 Systematic uncertainties

8.1 Luminosity uncertainty

The uncertainties on the integrated luminosity that is obtained from beam separation scans taken in whole 2015 and 2016 are ±2.1% and ±4.5% [23], respectively.

8.2 Theory uncertainties

The LHCHXSWG recommended scale and PDF uncertainties on SM single Higgs processes are documented in Ref [24], and they are used in the analysis as presented in Table 7.

Processes	+QCD Scale %	-QCD Scale %	$\pm PDF$ %	$\pm\alpha_s$ %
ggh	+7.6	-8.1	± 1.9	± 2.6
VBF	+0.4	-0.3	± 2.1	± 0.5
Wh	+0.5	-0.7	± 1.7	± 0.9
Zh	+3.8	-3.0	± 1.3	± 0.9
tth	+5.8	-9.2	± 3.0	± 2.0

Table 7: SM single Higgs scale and PDF uncertainties.

The LHCHXSWG recommended scale and PDF uncertainties on SM Higgs pair production are used in the analysis as presented in Table 8.

$\sqrt{s}$	$\sigma^{NNLO}_{gg\to hh}$	Scale	$\pm PDF$ %	$\pm\alpha_s$ %	EFT
13 TeV	33.41 fb	+4.3% -6.0%	±2.1%	±2.3%	±5%

Table 8: SM Higgs pair process (ggF) scale and PDF uncertainties, taken from Ref [25], only applied to the non-resonant analysis

Additional uncertainty of +2.1%/-2.0% applies to the $h \to \gamma\gamma$ branching ratio, and +1.5%/-1.5% to the $h \to WW$ branching ratio according to recommendations from Ref [26], since the final upper limits is set on $\sigma(gg \to hh)$ and $\sigma(gg \to H) \times BR(X \to hh)$.

see Table 9.

sampleName	full simulation(3jet)	MadGraph(3jet)	relative	full simulation(4jet)	MadGraph(4jet)	relative
ggH	0.0643791	0.0181966	-0.717353	0.021731	0.00512241	-0.764281
WH	0.19021	0.223821	0.176703	0.0727109	0.0695991	-0.0427966
ZH	0.186998	0.141362	-0.244044	0.068927	0.0751649	0.0905005

Table 9: theoretical

8.3 Object uncertainties

8.3.1 Leptons

8.3.2 Photons

8.3.3 Jets

8.3.4 *b*-tagging

8.4 Background modeling uncertainty

As discussed in 7.3, the yield of spurious signal is taken as the uncertainty of background modeling and it will be put into the final statistic model.

	non-resonant	260 GeV	300 GeV	400 GeV	500 GeV
upper limit(fb)	23.4	70.3	54.7	26.9	10.1

Table 10: summary of upper limit of all the mas point. No systematic is included now.

9 Statistical interpretation

The statistical procedure starts with the definition of the likelihood $\mathcal{L}$ defined as in Equation 2 for each category. The full likelihood is the product of the likelihood in all two categories.

$$
\begin{aligned}
\mathcal{L}_{cat}(N_s^{cat}, \theta) \propto \prod_{m_{\gamma\gamma}\in cat} \{ & \sum_{proc} (N_s^{cat}(\theta_{s,yield})^{cat}) \times f_s^{cat}(m_{\gamma\gamma}, \theta_{s,shape}^{cat}) \\
& + N_b^{cat} \times f_b^{cat}(m_{\gamma\gamma}, \theta_{b,shape}^{cat}) \\
& + N_{spurious}^{cat} \times \theta_{spurious}^{cat} \times f_s^{cat}(m_{\gamma\gamma}, \theta_{s,shape}^{cat}) \}
\end{aligned} \tag{2}
$$

The signal f_S and background f_B probability density functions (pdf) are the ones defined in the previous section 7. In the fit, the signal shapes, background shapes and background normalization are fixed and the signal normalization is left free.

θ denotes the nuisance parameters, including the background shape and normalization parameters and the systematics. The model defined in Equation 2 is modified to add new parameters to account for the systematics uncertainties, allowing the expected signal and SM background to vary within limits dictated by the estimations of these parameters in previous subsections.

The spurious signal is estimated as the uncertainties coming from the background modeling and it is implemented as an additional number of signal events.

The best fit values will be obtained by maximizing the likelihood 2 (or minimizing the function $-2ln(\mathcal{L})$).

A likelihood ratio based test statistic is used in the statistical analysis. It is defined as follows:

$$
\tilde{q}_\mu = \begin{cases} -2\ln\frac{\mathcal{L}(\mu,\hat{\hat{\theta}}(\mu))}{\mathcal{L}(0,\hat{\hat{\theta}}(0))} & \text{if } \hat{\mu} < 0 \\ -2\ln\frac{\mathcal{L}(\mu,\hat{\hat{\theta}}(\mu))}{\mathcal{L}(\hat{\mu},\hat{\theta})} & \text{if } 0 \le \hat{\mu} \le \mu \\ 0 & \text{if } \hat{\mu} > \mu \end{cases} \tag{3}
$$

where $\mathcal{L}$ stands for the likelihood function for the statistical model of the analysis, θ is the set of nuisance parameters that introduce the systematic uncertainties as mentioned above, and the parameter of interest (POI) μ is the cross section of non-resonant production or the cross section of resonant production times the branching ratio of $X \to hh$. Single hat stands for unconditional fit and double hat for conditional fit, i.e., POI μ is fixed to a certain value. With this test statistic, one derives the upper limits of the cross section for non-resonant production and the cross section times the branching ratio of $X \to hh$ for resonant production at 95% confidence level by using the CL_s method [27] under the asymptotic approximation [28]. The results are shown in Figure 25 and the numbers are summarized in Table 10. No systematics is included now.

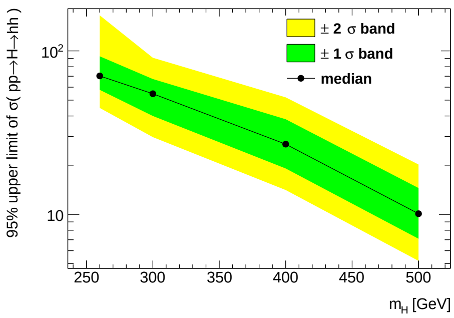

(a)

Figure 25: 95% upper limit of different mass point.

10 Unblinded result

11 Summary

References

[1] ATLAS Collaboration, *Observation of a new particle in the search for the Standard Model Higgs boson with the ATLAS detector at the LHC*, Phys. Lett. B **716** (2012) 1–29. http://www.sciencedirect.com/science/article/pii/S037026931200857X.

[2] CMS Collaboration, *Observation of a new boson at a mass of 125 GeV with the CMS experiment at the LHC*, Phys. Lett. B **716** (2012) 30–61. http://www.sciencedirect.com/science/article/pii/S0370269312008581.

[3] ATLAS Collaboration, *Measurements of Higgs boson production and couplings in diboson final states with the ATLAS detector at the LHC*, Phys.Lett. **B726** (2013) 88–119.

[4] The CMS Collaboration, *Combination of standard model Higgs boson searches and measurements of the properties of the new boson with a mass near 125 GeV*, CMS-PAS-HIG-13-005, CERN, Geneva, 2013. http://cdsweb.cern.ch/record/1542387.

[5] ATLAS and CMS Collaborations ATLAS-CONF-2015-044, Sep, 2015. https://atlas.web.cern.ch/Atlas/GROUPS/PHYSICS/CONFNOTES/ATLAS-CONF-2015-044/.

[6] S. Dawson, S. Dittmaier, and M. Spira, *Neutral Higgs-boson pair production at hadron colliders: QCD corrections*, Phys. Rev. **D58** (1998) 115012, arXiv:hep-ph/9805244 [hep-ph].

[7] J. Grigo, J. Hoff, K. Melnikov, and M. Steinhauser, *On the Higgs boson pair production at the LHC*, Nucl. Phys. **B875** (2013) 1, arXiv:1305.7340 [hep-ph].

[8] D. de Florian and J. Mazzitelli, *Higgs Boson Pair Production at Next-to-Next-to-Leading Order in QCD*, Phys.Rev.Lett. **111** (2013) 201801.

[9] H. E. Haber and G. L. Kane, *The search for supersymmetry: Probing physics beyond the standard model*, Phys. Rept. **117** (1985) 75.

[10] G. C. Branco, P. M. Ferreira, L. Lavoura, M. N. Rebelo, M. Sher, and J. P. Silva, *Theory and phenomenology of two-Higgs-doublet models*, Phys. Rept. **516** (2012) 1–102, arXiv:1106.0034 [hep-ph].

[11] ATLAS Collaboration, G. Aad et al., *Search For Higgs Boson Pair Production in the $\gamma\gamma b\bar{b}$ Final State using pp Collision Data at $\sqrt{s} = 8$ TeV from the ATLAS Detector*, Phys.Rev.Lett. **114** (2015) no. 8, 081802, arXiv:1406.5053 [hep-ex].

[12] ATLAS Collaboration, ATLAS Collaboration, *Search for Higgs boson pair production in the $b\bar{b}b\bar{b}$ final state from pp collisions at $\sqrt{s} = 8$ TeV with the ATLAS detector*, Eur. Phys. J. **C75** (2015) 412, arXiv:1506.00285 [hep-ex].

[13] CMS Collaboration, CMS Collaboration, *Search for resonant pair production of Higgs bosons decaying to two bottom quark-antiquark pairs in proton-proton collisions at 8 TeV*, Phys. Lett. **B749** (2015) 560, arXiv:1503.04114 [hep-ex].

[14] ATLAS Collaboration, G. Aad et al., *Searches for Higgs boson pair production in the $hh \to bb\tau\tau, \gamma\gamma WW^*, \gamma\gamma bb, bbbb$ channels with the ATLAS detector*, Phys. Rev. **D92** (2015) 092004, arXiv:1509.04670 [hep-ex].

[15] J. Alwall, M. Herquet, F. Maltoni, O. Mattelaer, and T. Stelzer, *MadGraph 5 : Going Beyond*, JHEP **06** (2011) 128, arXiv:1106.0522 [hep-ph].

[16] Web pages. F. Maltoni, Higgs pair production. https://cp3.irmp.ucl.ac.be/projects/madgraph/wiki/HiggsPairProduction, Dec 2013.

[17] S. Frixione and B. R. Webber, *Matching NLO QCD computations and parton shower simulations*, JHEP **06** (2002) 029, arXiv:hep-ph/0204244 [hep-ph].

[18] J. Grigo, J. Hoff, and M. Steinhauser, *Higgs boson pair production: top quark mass effects at NLO and NNLO*, Nucl. Phys. **B900** (2015) 412–430, arXiv:1508.00909 [hep-ph].

[19] J. Bellm et al., *Herwig++ 2.7 Release Note*, arXiv:1310.6877 [hep-ph].

[20] S. Gieseke, C. Rohr, and A. Siodmok, *Colour reconnections in Herwig++*, Eur. Phys. J. **C72** (2012) 2225, arXiv:1206.0041 [hep-ph].

[21] P. M. Nadolsky, H.-L. Lai, Q.-H. Cao, J. Huston, J. Pumplin, D. Stump, W.-K. Tung, and C. P. Yuan, *Implications of CTEQ global analysis for collider observables*, Phys. Rev. **D78** (2008) 013004, arXiv:0802.0007 [hep-ph].

[22] M. Cacciari, G. P. Salam, and G. Soyez, *The anti- k t jet clustering algorithm*, Journal of High Energy Physics **2008** (2008) no. 04, 063.

[23] *LuminosityForPhysics*, https://twiki.cern.ch/twiki/bin/viewauth/Atlas/LuminosityForPhysics.

[24] *CERN Yellow Report 4*, https://twiki.cern.ch/twiki/bin/view/LHCPhysics/CERNYellowReportPageAt13TeV.

[25] *LHC Higgs Cross Section HH Sub-group*, https://twiki.cern.ch/twiki/bin/view/LHCPhysics/LHCHXSWGHH#Current_recommendations_for_di_H.

[26] *LHC Higgs Cross Section Working Group*, https://twiki.cern.ch/twiki/bin/view/LHCPhysics/CERNYellowReportPageBR#Higgs_2_fermions.

[27] A. L. Read, *Presentation of search results: The CL(s) technique*, J.Phys. **G28** (2002) 2693–2704.

[28] G. Cowan et al., *Asymptotic formulae for likelihood-based tests of new physics*, Eur. Phys. J. **C71** (2011) 1554, arXiv:1007.1727 [physics.data-an].

Appendices

A Discussion on selection optimization

This section introduces another strategy considered in this analysis. It applies constrains on the invariant masses of the reconstructed on-shell W, off-shell W and the BSM Higgs, and optimizes the $pT_{\gamma\gamma}$ cuts similarly as Strategy 1.

A.1 Jet combination

The on-shell W boson can be reconstructed with different cobmination of the jets, as listed in Table 11. The corresponding match efficiency is listed in Table 12. The option that chooses the dijet system with its mass closest to W mass gives best mass resoultion and is therefore used here. The off-shell W candidate is reconstructed with the rest jets in the events. The invariant mass distribution of the dijet for signal samples with different resonance masses is shown in Figure 26. Figure 29 shows the 2D distribution of invariant mass of selected on-shell and off-shell W boson. From the plot, a rough W mass window cut, $|m_{on-shell\ W} - 80GeV| < 20GeV$ and $m_{off-shell\ W} < 80GeV$, is determined. After a further investigation, it is found that this constraint is not helpful to the sinificance, so this constraint is not introduced at the end. Figure 27 shows the distribution of m_{jj} and Figure 28 shows the scan.

method to select on-shell W	description
leading 4 jets	select the 4 leading jets. take leading two jets as on-shell W and subleading two jets as off-shell W.
leading and closest	select a leading jet and another closest as on-shell W boson
dijet mass closest to W mass	select dijet which invariant mass is closest to W mass
closest dijet	select the closest dijet

Table 11: method description of W boson reconstruction

A.2 Mass window of diphoton plus jet system

In the resonant search, mass spectrum of diphoton plus 3 or 4 jets can indicate the mass of capital Higgs, so a mass constrain is performed in resonant analysis. The mass distribution of $\gamma\gamma$+3(4) jets is shown in Figure 30 after jet selection and W mass constrain. A mass window which contains 85 % signal events is defined in Figure 31.

A.3 $pT_{\gamma\gamma}$ cut

For both resonant and non-resonant search, $pT_{\gamma\gamma}$ has good separation power. Its distribution is shown in Figure 4. A scan on $pT_{\gamma\gamma}$ is performed to determine the best cut value for resonant and non-resonant

!h

method to selection on-shell W	260	300	400	500	non-res
truth match	0.385	0.375	0.442	0.498	0.489
leading di-jet	0.060	0.052	0.081	0.122	0.110
dijet mass closest to W mass	0.103	0.108	0.159	0.185	0.172
leading jet and closest	0.015	0.026	0.054	0.090	0.107
closest dijet	0.004	0.011	0.034	0.062	0.076

Table 12: This table shows match efficiency of different method. Truth means that ΔR between reco jet and truth jet is smaller than 0.4. Method of ”dijet mass closest to W mass ” has the best match efficiency and the efficiency is increasing as mass increases. The selection is inclusive diphoton, lepton veto, bjet veto and at least 4 central jets.

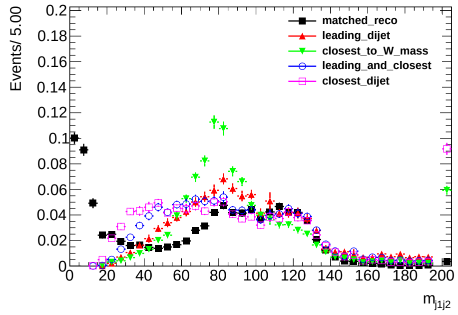

(a) 3 jet category of non-resonnat

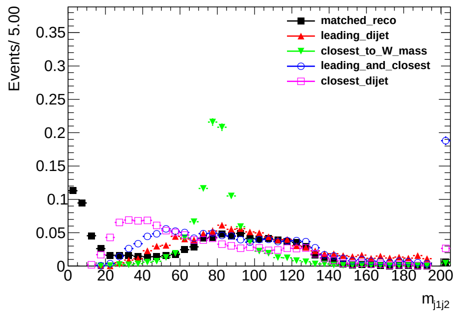

(b) 4 jet category of non-resonant

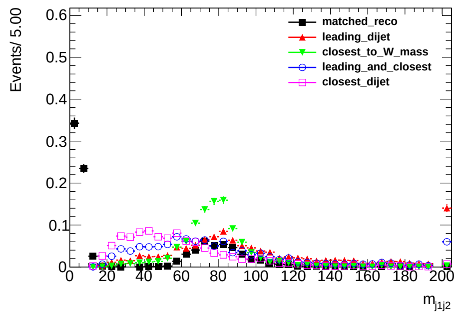

(c) 3 jet category of m_H = 260 GeV

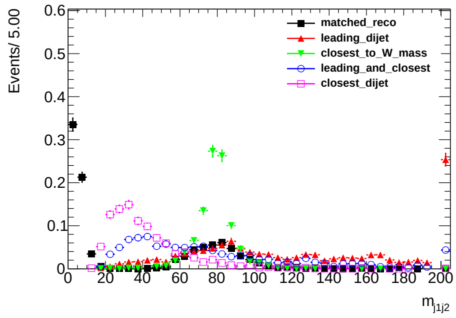

(d) 4 jet category of m_H = 260 GeV

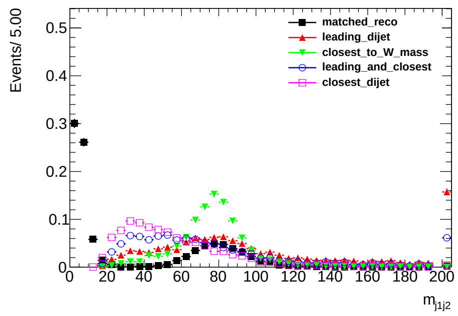

(e) 3 jet category of m_H = 300 GeV

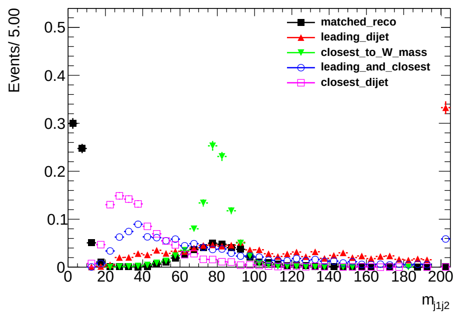

(f) 4 jet category of m_H = 300 GeV

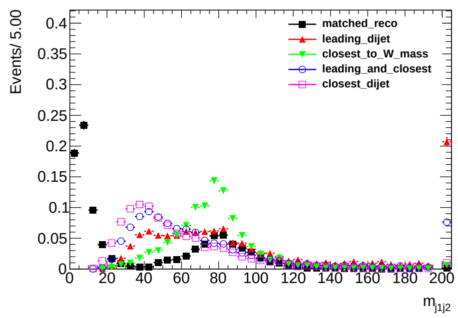

(g) 3 jet category of m_H = 400 GeV

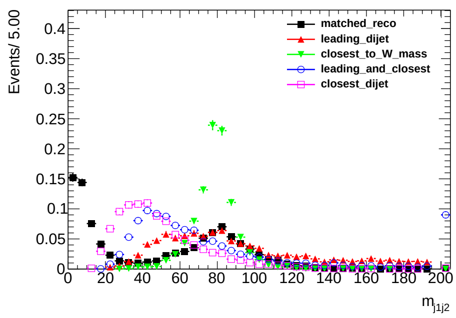

(h) 4 jet category of m_H = 400 GeV

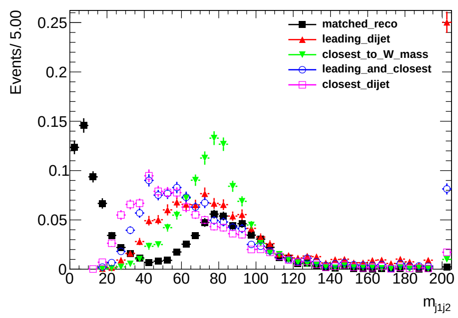

(i) 3 jet category of m_H = 500 GeV

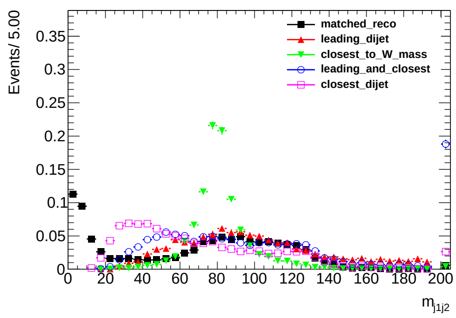

(j) 4 jet category of m_H = 500 GeV

Figure 26: invariant mass distribution of on-shell W candidate in different signal samples. The peak at 0

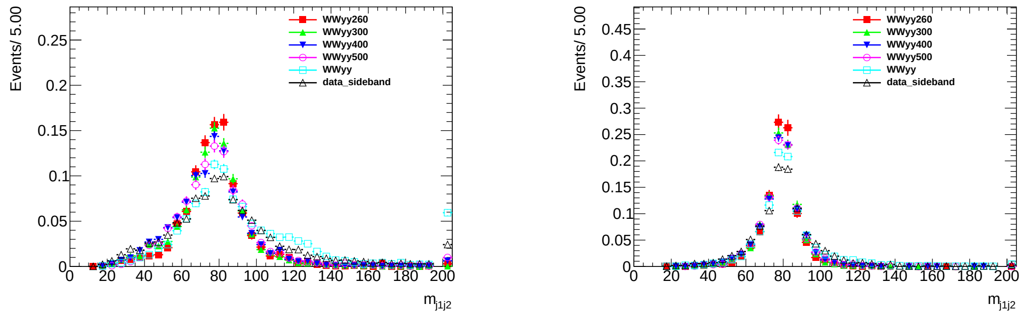

(a) 3 jet category

(b) 4 jet category

Figure 27: Data/MC comparison of m_{jj} closest to W mass shows very poor separation power.

	non-res		260 GeV		300 GeV		400 GeV		500 GeV	
mass window [GeV]	-	-	[205, 455]	[250, 560]	[240, 480]	[265, 600]	[315, 580]	[355, 685]	[415, 700]	[430, 775]
$pT_{\gamma\gamma}[GeV]$ cut	> 155	> 155	< 55	< 70	> 40	> 25	> 130	> 120	> 175	> 170
signal yield	0.48	0.64	0.43	0.24	0.50	0.37	0.48	0.48	0.51	0.55
SM Higgs	13.12	7.72	6.73	2.00	18.18	7.00	7.88	6.46	4.10	2.70
continuum	85.82	64.28	546	177	754	293	81	53	28	19
significance	0.048	0.076	0.018	0.018	0.018	0.022	0.044	0.065	0.089	0.139
combined significance	0.090		0.025		0.028		0.077		0.166	

Table 13: summary of selection, yield and significance

search. The expected signifcance calculated with expected signal yield, SM Higgs yield and continuum background yield in the scan using Equation 1 is shown in Figure 32, Figure 33, Figure 34, Figure 35, Figure 36 for different signal models. The final optimization cuts and all the expected numbers are listed in Table 13.

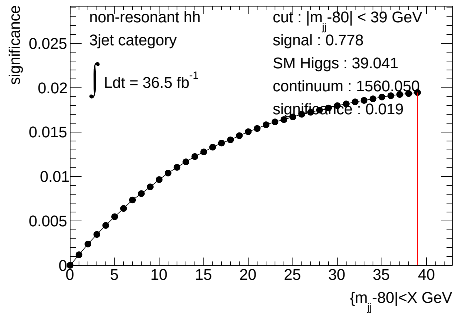

(a) 3 jet category of non-resonant

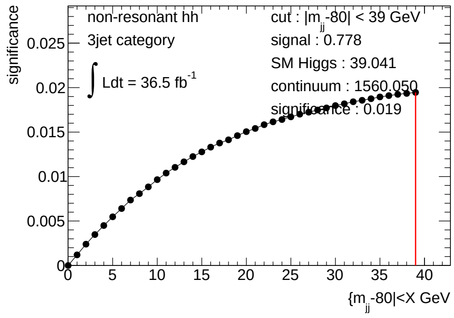

(b) 4 jet category of non-resonant

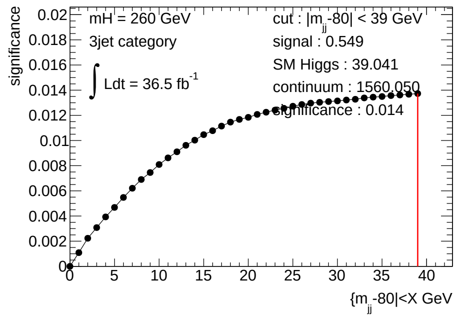

(c) 3 jet category of $m_H = 260GeV$

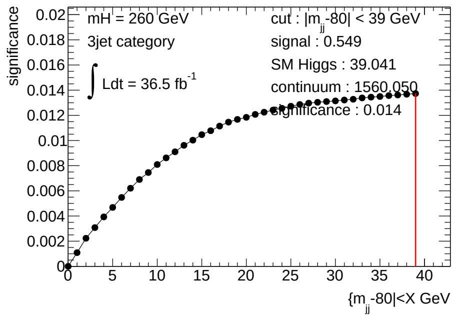

(d) 4 jet category of $m_H = 260GeV$

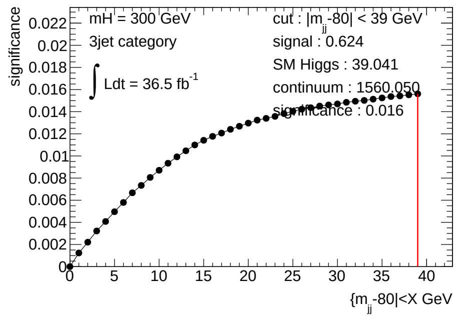

(e) 3 jet category of $m_H = 300GeV$

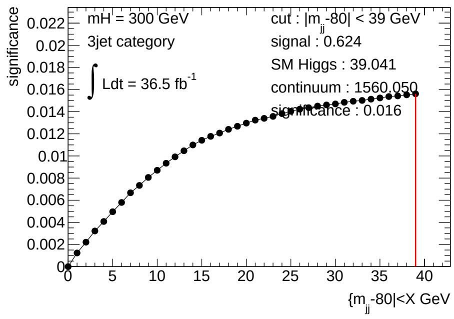

(f) 4 jet category of $m_H = 300GeV$

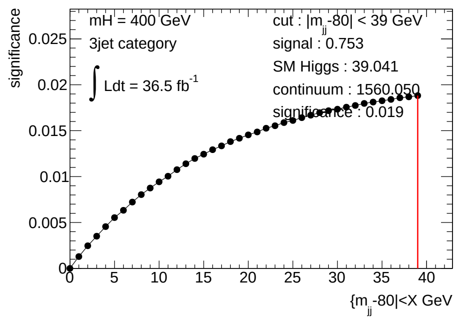

(g) 3 jet category of $m_H = 400GeV$

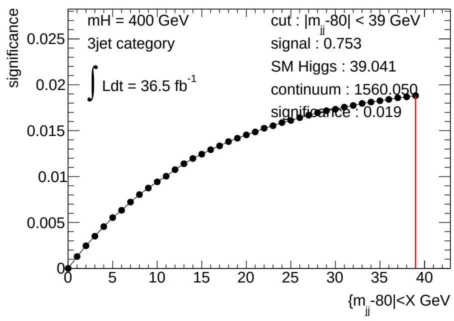

(h) 4 jet category of $m_H = 400GeV$

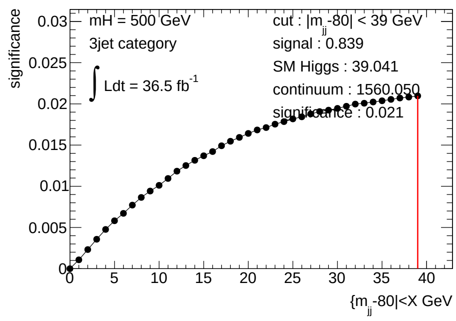

(i) 3 jet category of $m_H = 500GeV$

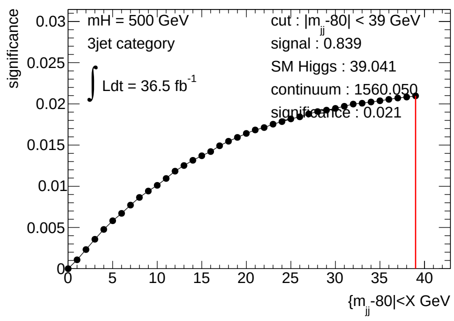

(j) 4 jet category of $m_H = 500GeV$

Figure 28: The constraint of m_{jj} mass window can not improve the significance.

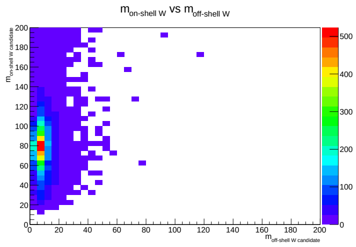

(a) 3 jet category of data sideband

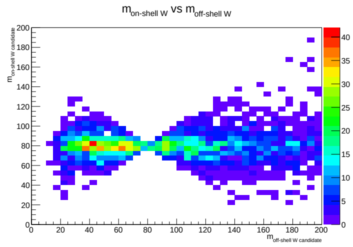

(b) 4 jet category of data sideband

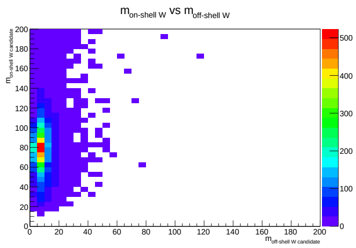

(c) 3 jet category of non-resonant

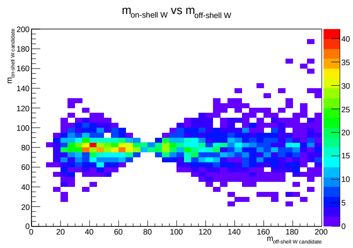

(d) 4 jet category of non-resonant

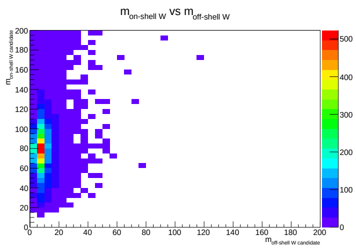

(e) 3 jet category of m_H = 260 GeV

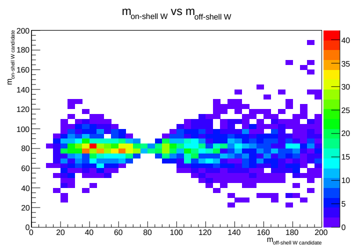

(f) 4 jet category of m_H = 260 GeV

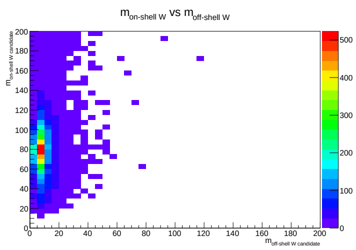

(g) 3 jet category of m_H = 300 GeV

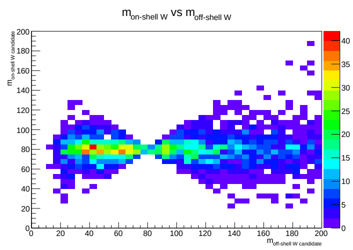

(h) 4 jet category of m_H = 300 GeV

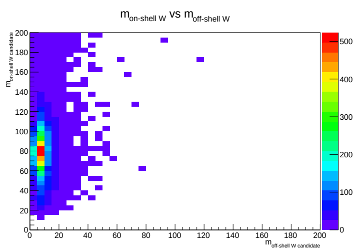

(i) 3 jet category of m_H = 400 GeV

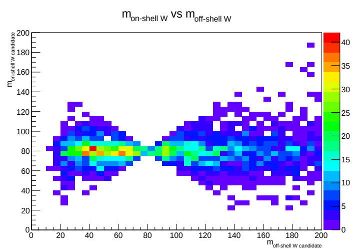

(j) 4 jet category of m_H = 400 GeV

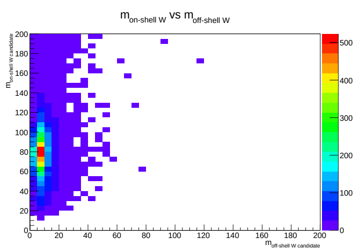

(k) 3 jet category of m_H = 500 GeV

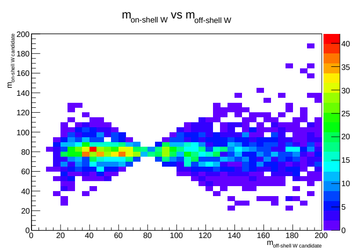

(l) 4 jet category of m_H = 500 GeV

Figure 29: 2D distribution of selected on-shell W mass vs off-shell W mass

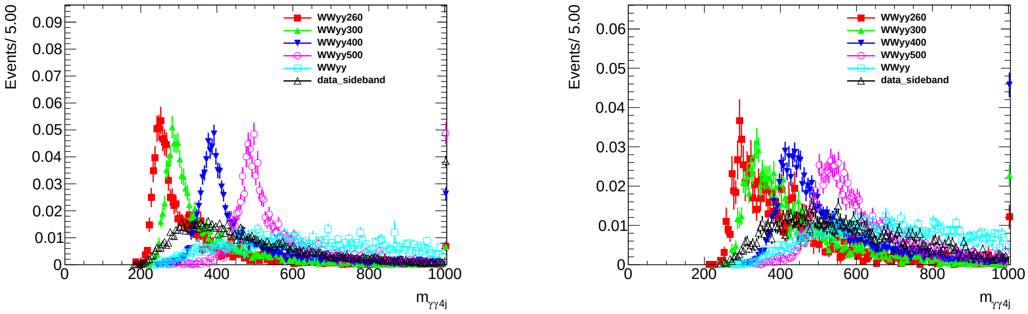

(a) leading jet of on-shell W

(b) subleading jet of on-shell W

Figure 30: pT of four signal jets at truth level

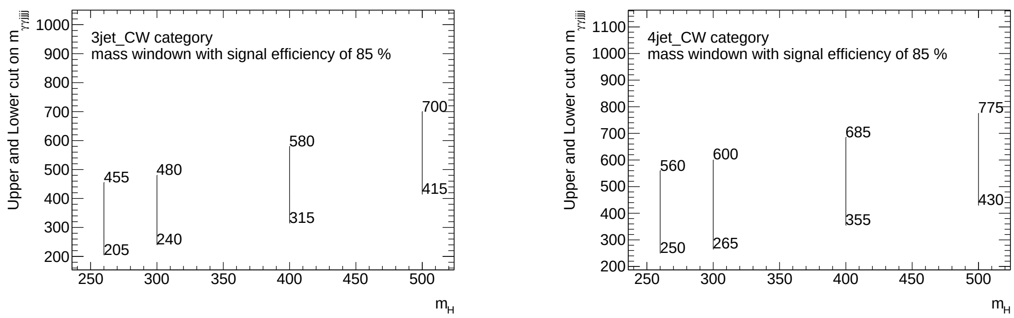

(a) mass window of 3 jet category

(b) mass window of 4 jet category

Figure 31: mass window containing 85 % signal events

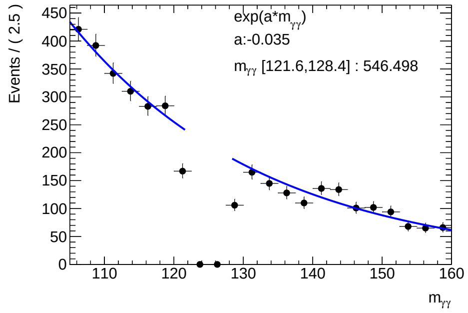

(a) data sideband fit of 3 jet category

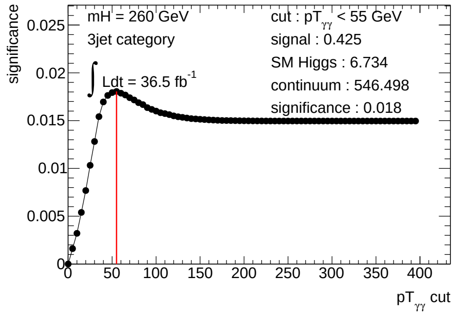

(b) data sideband fit of 4 jet category

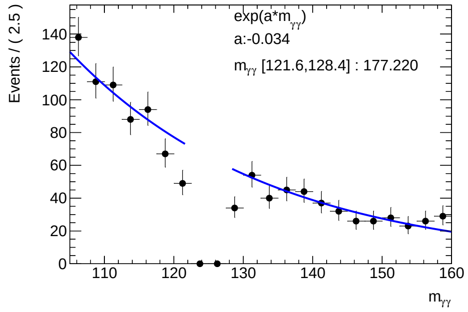

(c) cut scan of 3 jet category

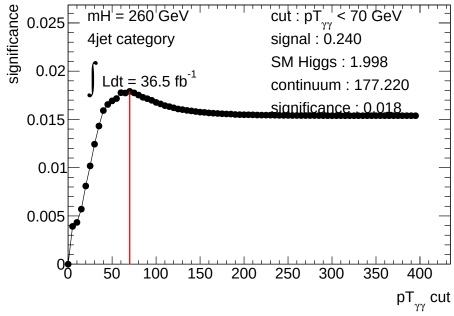

(d) cut scan of 4 jet category

Figure 32: scan the $pT_{\gamma\gamma}$ cut and plot the data sideband fit for m_H = 260 GeV.

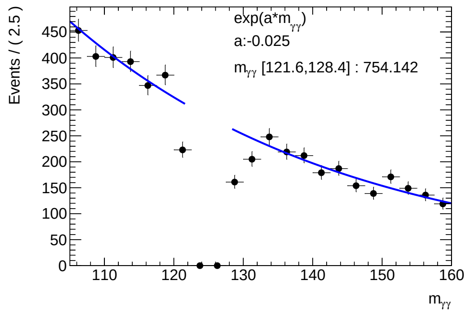

(a) data sideband fit of 3 jet category

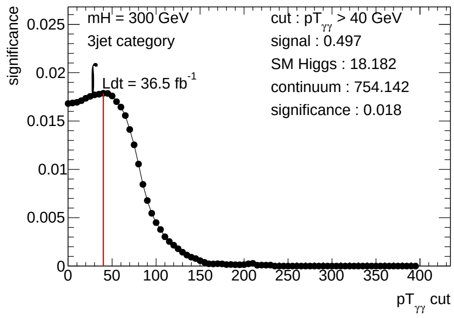

(b) data sideband fit of 4 jet category

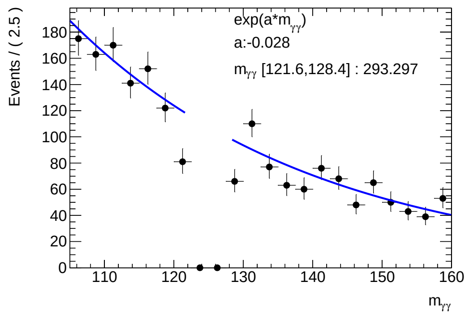

(c) cut scan of 3 jet category

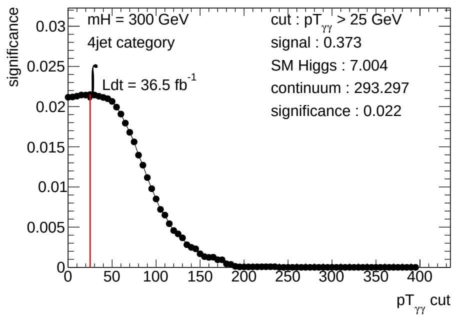

(d) cut scan of 4 jet category

Figure 33: scan the $pT_{\gamma\gamma}$ cut and plot the data sideband fit for m_H = 300 GeV.

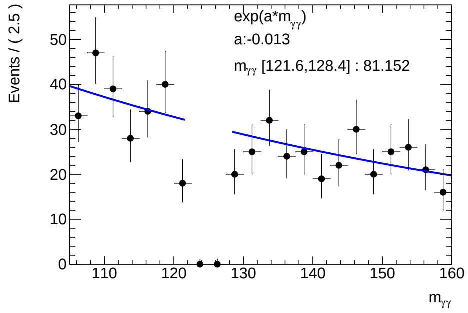

(a) data sideband fit of 3 jet category

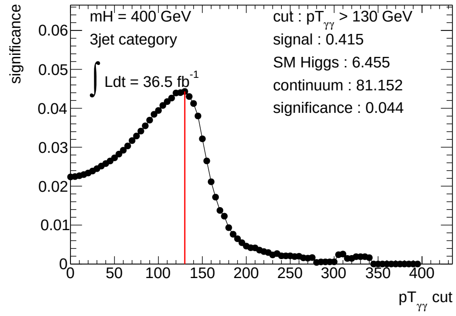

(b) data sideband fit of 4 jet category

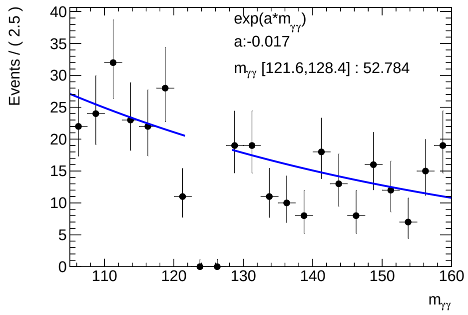

(c) cut scan of 3 jet category

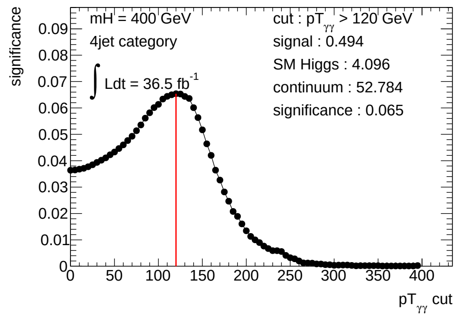

(d) cut scan of 4 jet category

Figure 34: scan the $pT_{\gamma\gamma}$ cut and plot the data sideband fit for m_H = 400 GeV.

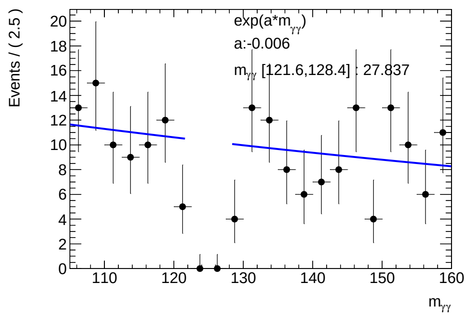

(a) data sideband fit of 3 jet category

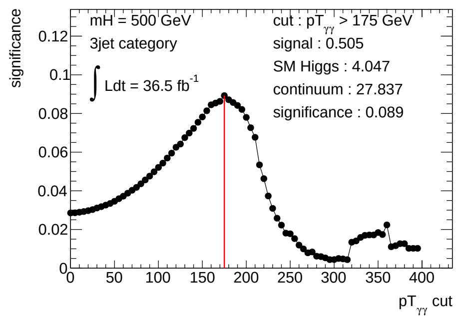

(b) data sideband fit of 4 jet category

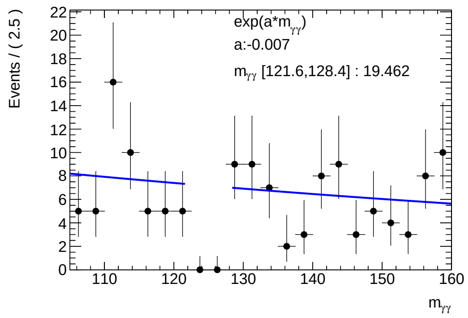

(c) cut scan of 3 jet category

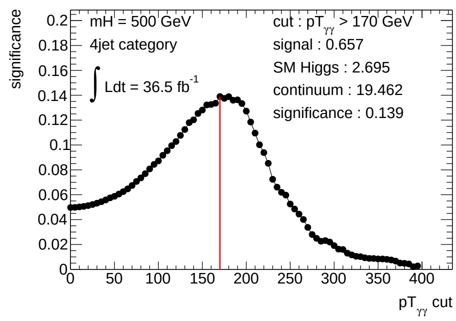

(d) cut scan of 4 jet category

Figure 35: scan the $pT_{\gamma\gamma}$ cut and plot the data sideband fit for m_H = 500 GeV.

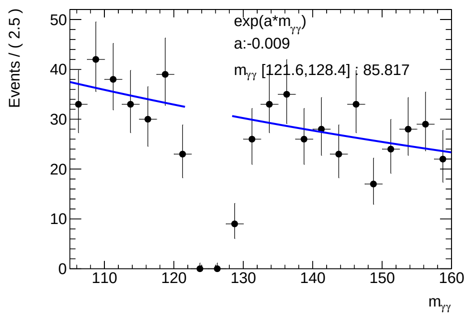

(a) data sideband fit of 3 jet category

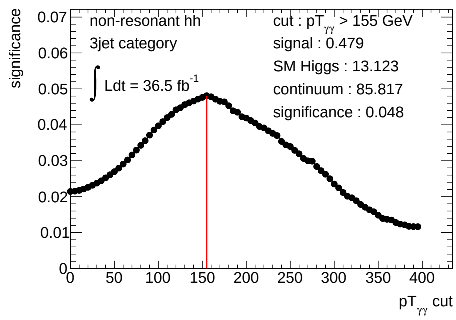

(b) data sideband fit of 4 jet category

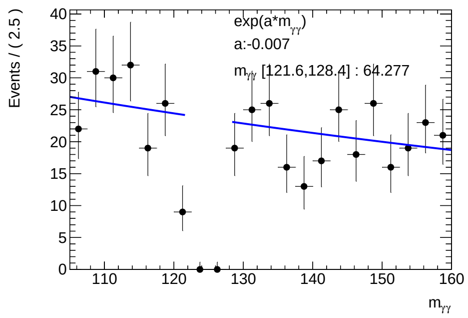

(c) cut scan of 3 jet category

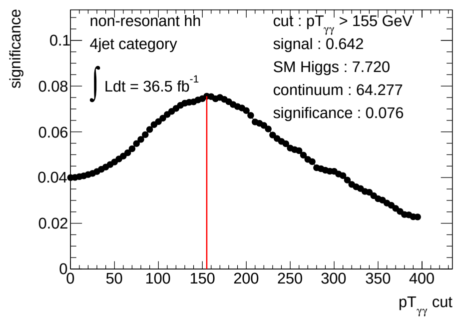

(d) cut scan of 4 jet category

Figure 36: scan the $pT_{\gamma\gamma}$ cut and plot the data sideband fit for non-resonant.